ARTICLES
https://doi.org/10.1038/s41564-021-00866-3
nature microbiology

Check for updates

The *Salmonella* effector protein SopD targets Rab8 to positively and negatively modulate the inflammatory response

Huan Lian[1,4], Kun Jiang[2,4], Ming Tong[2,4], Zhe Chen[2], Xiaoyu Liu[2], Jorge E. Galán[1]✉ and Xiang Gao[2,3]✉

The food-borne bacterial pathogen *Salmonella* Typhimurium uses a type III protein secretion system to deliver multiple proteins into host cells. These secreted effectors modulate the functions of host cells and activate specific signalling cascades that result in the production of pro-inflammatory cytokines and intestinal inflammation. Some of the *Salmonella*-encoded effectors counteract this inflammatory response and help to preserve host homeostasis. Here, we demonstrate that the *Salmonella* effector protein SopD, which is required for pathogenesis, functions to both activate and inhibit the inflammatory response by targeting the Rab8 GTPase, which is a negative regulator of inflammation. We show that SopD has GTPase-activating protein activity for Rab8 and, therefore, inhibits this GTPase and stimulates inflammation. We also show that SopD activates Rab8 by displacing it from its cognate guanosine dissociation inhibitor, resulting in the stimulation of a signalling cascade that suppresses inflammation. We solved the crystal structure of SopD in association with Rab8 to a resolution of 2.3 Å, which reveals a unique contact interface that underlies these complex interactions. These findings show the remarkable evolution of a bacterial effector protein to exert both agonistic and antagonistic activities towards the same host cellular target to modulate the inflammatory response.

The pathogen *Salmonella* Typhimurium stimulates a potent inflammatory response in the intestinal epithelium through the activities of its type III secretion (TTS) effector proteins SopE, SopE2 and SopB[1–5]. These effector proteins stimulate these responses independent of innate immune receptors by redundantly targeting the Rho-family GTPase Cdc42 (refs. [1–5]). The stimulation of Cdc42 results in the activation of its effector p21-activated protein kinase 1 (PAK1), leading to the non-canonical recruitment of tumour necrosis factor receptor associated factor 6 (TRAF6) and mitogen-activated protein kinase kinase kinase 7 (TAK1), with the subsequent stimulation of NF-κB inflammatory signalling[4]. Additional effector proteins contribute to the enhancement of the inflammatory response by targeting other pro-inflammatory signalling pathways[6–8]. The stimulation of an inflammatory response is central to pathogenicity, enabling *S.* Typhimurium to compete against the resident microbiota and to acquire the nutrients and electron acceptors that sustain its replication[9,10]. However, the preservation of host homeostasis is equally important in the *Salmonella*–host interaction. As a consequence, in a remarkable 'yin and yang', *Salmonella* has evolved a subset of TTS effector proteins that oppose the action of its agonistic effector-protein counterparts. For example, to counteract the action of the Rho-family GTPase agonists SopE, SopE2 and SopB, *Salmonella* delivers the effector protein SptP, which exhibits potent GTPase-activating protein (GAP) activity towards the same Rho-family GTPases[11]. Furthermore, to counteract the pro-inflammatory effectors that activate NF-κB signalling, *Salmonella* delivers three effector proteins with highly specific protease activity towards the NF-κB transcription factors RelA and RelB[12].

Previous studies have shown that the *Salmonella* TTS effector protein SopD synergizes with other effectors to stimulate inflammation in an animal model of infection[13,14]. However, the mechanism by which this effector carries out this function is unknown. In this Article, we show that SopD exerts its activity by targeting the Rab-family GTPase Rab8. Recent studies have shown that Rab8 negatively regulates the inflammatory response mediated through Toll-like receptors (TLRs)[15–17]. We found that, through its GAP activity, SopD antagonizes Rab8, therefore enhancing the inflammatory response to *Salmonella*. Furthermore, through an additional activity that results in the displacement of Rab8 from its cognate guanosine dissociation inhibitor (GDI), SopD activates this GTPase, therefore countering the inflammatory response. Thus, this bifunctional effector protein can both activate and inhibit Rab8-mediated signalling to stimulate and antagonize the inflammatory response induced by *Salmonella*.

Results

SopD is a GAP for Rab8. SopD exhibits significant amino acid sequence similarity to the related *Salmonella* effector protein SopD2 (Supplementary Fig. 1)[18], which neutralizes a Rab32-dependent cell intrinsic host defence mechanism by targeting this GTPase with its GAP activity[19]. Notably, a critical arginine residue in SopD2, Arg315, which is essential for its GAP catalytic activity, is conserved in SopD (Supplementary Fig. 1). However, SopD is unable to complement a Δ*sopD2* mutant for its ability to neutralize the Rab32 pathogen restriction mechanism[19]. Consistent with this finding, we found that SopD did not show any measurable GAP activity towards Rab32 (Fig. 1a). However, we found that, of the 24 additional Rab

[1]Department of Microbial Pathogenesis, Yale University School of Medicine, New Haven, CT, USA. [2]State Key Laboratory of Microbial Technology, Shandong University, Qingdao, China. [3]School of Life Sciences, Shandong University, Qingdao, China. [4]These authors contributed equally: Huan Lian, Kun Jiang, Ming Tong. ✉e-mail: jorge.galan@yale.edu; xgao@email.sdu.edu.cn

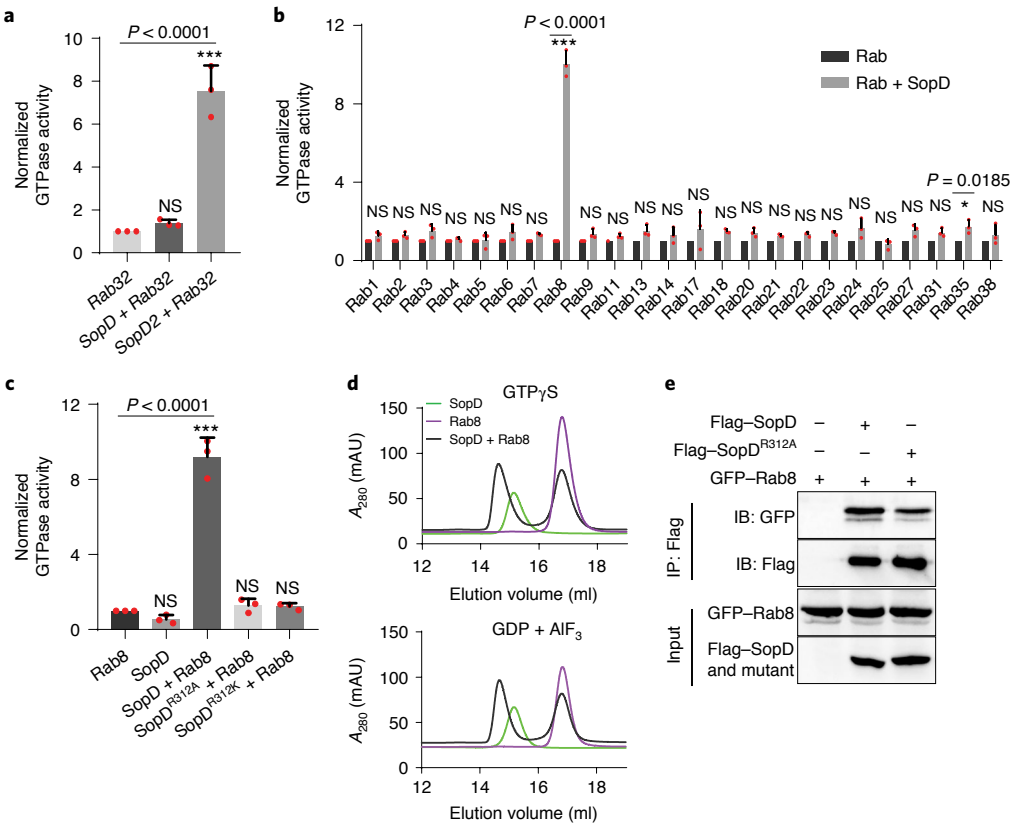

Fig. 1 | SopD is a GAP for Rab8. a, SopD lacks GAP activity towards Rab32. Purified Rab32 was incubated alone or in the presence of purified SopD or SopD2, as indicated, and the intrinsic GTPase activity was measured (Methods). **b**, GAP activity of SopD towards Rab-family GTPases. Purified Rab GTPases were incubated alone or in the presence of purified SopD, and the intrinsic GTPase activity was measured (Methods). **c**, SopD GAP activity towards Rab8 requires a critical arginine residue. Purified Rab8$^{1–183}$ was incubated alone or in the presence of purified SopD or the indicated mutants, and the intrinsic GTPase activity was measured (Methods). For **a**–**c**, data are the mean ± s.d. ratio of GTPase activity observed in the presence or absence of SopD from three independent experiments. Statistical analysis was performed using one-way analysis of variance (ANOVA) with Dunnett's method (**a** and **c**) and two-way ANOVA using Sidak's multiple-comparisons test (**b**); NS, not significant ($P > 0.05$); $^{*}P < 0.05$, $^{***}P < 0.001$. **d**, Size-exclusion chromatography profiles of the SopD–Rab8 complex. Rab8$^{1–183}$ preloaded with GTPγS or GDP + AlF_3 was incubated with SopD, and subsequently analysed using size-exclusion chromatography in a Superdex 200 increase column. A_{280}, absorbance at 280 nm. **e**, Co-immunoprecipitation analysis to detect the interaction between SopD and SopD^{R312A} and Rab8. HEK293T cells were transiently cotransfected with plasmids expressing GFP–Rab8 along with plasmids expressing Flag–SopD, Flag–SopD^{R312A} or an empty vector. Cell lysates were analysed using co-immunoprecipitation (IP) with anti-Flag and western immunoblotting (IB) with anti-GFP and anti-Flag antibodies. For **d** and **e**, experiments were conducted at least three times with equivalent results.

GTPases tested, SopD showed robust GAP activity towards only Rab8 (Fig. 1b). Similar to SopD2 (ref. [19]), the GAP activity of SopD was strictly dependent on the Arg312 residue, as the SopD^{R312A} and SopD^{R312K} mutants did not show any measurable GAP activity towards Rab8 (Fig. 1c). We found that SopD was able to form a complex with Rab8 (Fig. 1d) but we were unable to detect a stable complex between Rab8 and SopD2, which also exhibits GAP activity towards Rab8 (Extended Data Fig. 1)[19]. Furthermore, transient transfection experiments showed that both wild-type SopD and the catalytic mutant SopD^{R312A} were able to form a complex with Rab8 in vivo (Fig. 1e). These results indicate that, similar to its homologue SopD2, the bacterial effector SopD is also a GAP for a Rab GTPase but with different specificity.

SopD enhances pro-inflammatory signalling by antagonizing Rab8 through its GAP activity. Innate immune receptors are most often 'wired' to anti-inflammatory pathways that help the recovery of host homeostasis after an inflammatory response[20–25]. Rab8 has been linked to one such anti-inflammatory pathway downstream of TLRs resulting in the recruitment of phosphoinositide 3-kinase (PI3K), Akt activation and the biasing of cytokine production towards an anti-inflammatory program[15–17]. We investigated the potential role of Rab8 in *Salmonella*-induced inflammatory signalling. We examined whether, similar to lipopolysaccharide (LPS) stimulation[15], Rab8 could also be recruited to the membrane ruffles stimulated by *S.* Typhimurium by delivering a subset of TTS effector proteins[3,26,27]. We found that Rab8 was robustly recruited to the *Salmonella*-induced membrane ruffles, although recruitment did not require the presence of the effector protein SopD (Extended Data Fig. 2). As Henle 407 cells do not respond to LPS stimulation, these results indicate that, at least in these cells, the *Salmonella*-induced recruitment of Rab8 to membrane ruffles is independent of LPS.

There are two isoforms of RAB8, RAB8A and RAB8B, which exhibit significant (83%) amino-acid sequence identity and are thought to have some overlapping functions[28]. We compared the ability of *S.* Typhimurium to stimulate Akt and NF-κB signalling in wild-type, and RAB8A-, RAB8B- and RAB8A/RAB8B-deficient cell lines generated using CRISPR–Cas9-mediated genome editing (Supplementary Fig. 2). Although we detected no differences in NF-κB signalling after *S.* Typhimurium infection, we found significantly reduced levels of Akt phosphorylation in both Raw264.7 and HT29 RAB8A-deficient cell lines (Fig. 2a and Extended Data Fig. 3) despite equal levels of bacterial invasion (Supplementary Fig. 3). Consistent with these observations, in RAB8A-deficient

cells infected with *S.* Typhimurium, we found a significant reduction in the levels of mRNA encoding the anti-inflammatory cytokine IL-10 and an increase in the levels of mRNA encoding the pro-inflammatory cytokines IL-1β and TNFα (Fig. 2b). Although the observed changes were not as pronounced as those observed in the absence of RAB8A, the absence of RAB8B resulted in a decrease in Akt activation, a decrease in the levels of mRNA encoding the anti-inflammatory cytokine IL-10, and an increase in the levels of mRNA encoding the pro-inflammatory cytokines IL-1β and TNFα after *S.* Typhimurium infection (Fig. 2c and Extended Data Fig. 3). However, the absence of RAB8A and RAB8B resulted in a more pronounced decrease in Akt activation after *S.* Typhimurium infection as well as more significant changes in *Il10, Il1b and Tnf* mRNA levels (Fig. 2d and Extended Data Fig. 3). These results indicate that both RAB8A and RAB8B redundantly participate in *Salmonella*-induced inflammatory signalling, although RAB8A seems to have a more prominent role.

Next, we tested the effect of the expression of SopD on LPS-mediated inflammatory signalling. We found that expression of SopD led to significant inhibition of LPS-stimulated Akt activation, although it did not affect NF-κB and MAP kinase signalling (Fig. 2e, Extended Data Fig. 4 and Supplementary Fig. 4). More importantly, expression of SopD resulted in a shift towards a pro-inflammatory cytokine profile with an increase in the production of mRNA encoding the pro-inflammatory cytokines IL-1β and TNFα and a decrease in the production of mRNA encoding the anti-inflammatory cytokine IL-10 (Fig. 2f). The SopD-mediated modulation of LPS signalling was strictly dependent on its GAP activity, as the expression of the catalytic mutant SopD^{R312A} did not inhibit LPS-mediated signalling (Fig. 2e,f and Extended Data Fig. 4). Taken together, these results indicate that, through its Rab8 GAP activity, SopD has the ability to enhance *Salmonella*-induced inflammation by interfering with a negative regulatory mechanism that is linked to a pro-inflammatory signalling pathway.

Previous studies have shown that Rab8-dependent LPS-mediated Akt activation and the resulting anti-inflammatory response requires PI3K[15–17]. Furthermore, *S.* Typhimurium has been shown to activate Akt by stimulating phosphoinositide fluxes through the delivery of its TTSS effector protein SopB[29,30]. We found that, similar to LPS stimulation, the *S.* Typhimurium-induced Akt activation in both Raw264.7 macrophages and HT29 cells also required PI3K (Extended Data Fig. 5a). The addition of increasing concentrations of wortmannin, a specific PI3K inhibitor, resulted in a progressive inhibition of *Salmonella*-induced Akt activation. Importantly, the addition of the PI3K inhibitor resulted in an increase in the levels of mRNA encoding the pro-inflammatory cytokines IL-1β and TNFα and a decrease in the levels of mRNA encoding the anti-inflammatory cytokine IL-10 (Extended Data Fig. 5b).

Taken together, these results implicate both Rab8a and Rab8b as well as PI3K in the negative modulation of the inflammatory response to *S.* Typhimurium. Importantly, these results suggest a mechanism by which the effector protein SopD, through its GAP activity, enhances the inflammatory response to *Salmonella* by inhibiting Rab8.

The crystal structure of SopD in complex with Rab8 reveals a functional interface that suggests the presence of additional activity. To better define their functional interface, we solved the crystal structure of SopD in complex with RAB8A at a resolution of 2.3 Å. The complex is formed by one molecule each of SopD and Rab8 and is arranged in a V-shaped architecture, with each of the molecules forming one leg of the V (Fig. 3a and Supplementary Fig. 5). The interface between SopD and Rab8 buries a surface area of ~1,000 Å^2. Close inspection of this interface revealed structural elements in Rab8 that contain Rab-family-specific (RabF) and Rab-subfamily-specific (RabSF) motifs[31,32], which form a hand-in-hand interface with the α11 helix, β4/β5 anti-parallel sheets, as well as loops L_A, L_B and L_C in SopD (Fig. 3a,b and Supplementary Fig. 5). SopD engages the RabF motif through hydrophobic interactions between its residues Val 237 and Ala 242, and the Rab8 residues Ile 43, Phe 45 and Trp 62. Furthermore, polar interactions between Lys 58, Thr 74 and Arg 79 in Rab8, and Gln 107, Ser 138, Glu 240, Tyr 278 and Glu 293 in SopD, as well as two water-mediated hydrogen bonds between Gln 60 in Rab8 and Lys 285 and Asp 289 in SopD further stabilize the complex (Fig. 3b,c). Additional interactions involve residues within the RabSF motif in Rab8 (Tyr 5, Tyr 7 and Leu 177) and Glu 293, Val 290 and Phe 287 in SopD, in addition to hydrophobic interactions between Ala 76 in the switch-II region of Rab8 and Met 139 in SopD, Met 82 in Rab8 and Met 286 in SopD, as well as one direct hydrogen bond between Lys 46 in Rab8 and Gln 238 in SopD (Fig. 3b,c).

Surprisingly and contrary to what its GAP activity would predict, the Rab8–SopD interface does not position the catalytic Arg 312 residue of SopD in close proximity to the nucleotide-binding pocket of Rab8 (Fig. 3a). Rather, the arrangement of SopD in the complex positions its Arg 312 catalytic residue on the opposite side of its Rab8-interacting surface. Furthermore, although a clear electron density for GDP and Mg^{2+} was apparent, no electron density corresponding to ALF_3 could be discerned in the structure, despite its presence in the crystallization buffer (Fig. 3a and Supplementary Fig. 6). This is consistent with the observation that SopD was able to form a complex with GDP-loaded Rab8 (Extended Data Fig. 6).

The overall structure of SopD in the complex is virtually identical to its previously determined apo structure[33], with a root mean squared deviation of 0.499 Å over 255 Cα atoms (Supplementary Fig. 7). Structural alignment of Rab8 as it appears in complex with SopD with either the GDP-bound Rab8 from the Rab8–rabin8 complex (Protein Data Bank (PDB): 4LHY) or GDP-bound inactive Rab8 (PDB: 4LHW)[34] revealed marked conformational changes in the switch-I and -II as well as the RabSF1 regions of Rab8 that

Fig. 2 | SopD enhances pro-inflammatory signalling by antagonizing RAB8 through its GAP activity. a–d, The effects of RAB8A or RAB8B deficiency on *S.* Typhimurium-induced Akt and NF-κB signalling. Control and RAB8A (**a**), RAB8B (**c**) or RAB8A/RAB8B- (**d**) deficient Raw264.7 or HT29 (as indicated) cells were infected with wild-type *S.* Typhimurium with a multiplicity of infection (m.o.i.) of 2 and 10, respectively. At the indicated times after infection, the levels of phosphorylated AKT, the total levels of IκBα and the mRNA levels of the indicated cytokines were quantified using immunoblotting (**a**,**c**,**d**) and quantitative PCR (qPCR) analysis (**b**) of the indicated cells. Data are mean ± s.d. of three independent determinations. Statistical analysis was performed using unpaired two-sided *t*-tests; $^*P < 0.05$, $^{**}P < 0.01$, $^{***}P < 0.001$; NS, not significant ($P > 0.05$). The quantification of the immunoblots is shown in Extended Data Fig. 3. **e**,**f**, The effect of the expression of SopD or its catalytic mutant SopD^{R312A} on LPS-induced Akt, p70S6K, Erk1/2, p38 MAP and NF-κB signalling and cytokine gene expression. **e**, Raw264.7 cells stably expressing HA-tagged SopD or its GAP-deficient mutant SopD^{R312A} were treated with LPS (100 ng ml^{-1}) for the indicated times, lysed and analysed using immunoblotting with antibodies specific for phosphorylated Akt, p70S6K, p38 and Erk1/2, as well as antibodies against IκBα and β-actin (as a loading control). The quantification of the western blot analyses is shown. A repetition of this experiment is shown in Supplementary Fig. 4. Data are mean ± s.d. of three independent determinations. **f**, Alternatively, Raw264.7 cells stably expressing HA-tagged SopD or its GAP-deficient mutant SopD^{R312A} were treated with LPS (50 ng ml^{-1}) for the indicated times and the mRNA levels of the indicated cytokines were quantified using qPCR at the indicated times after treatment. Data are mean ± s.d. of three independent determinations. Statistical analysis was performed using unpaired two-sided *t*-tests; $^*P < 0.05$, $^{**}P < 0.01$, $^{***}P < 0.001$; NS, not significant ($P > 0.05$).

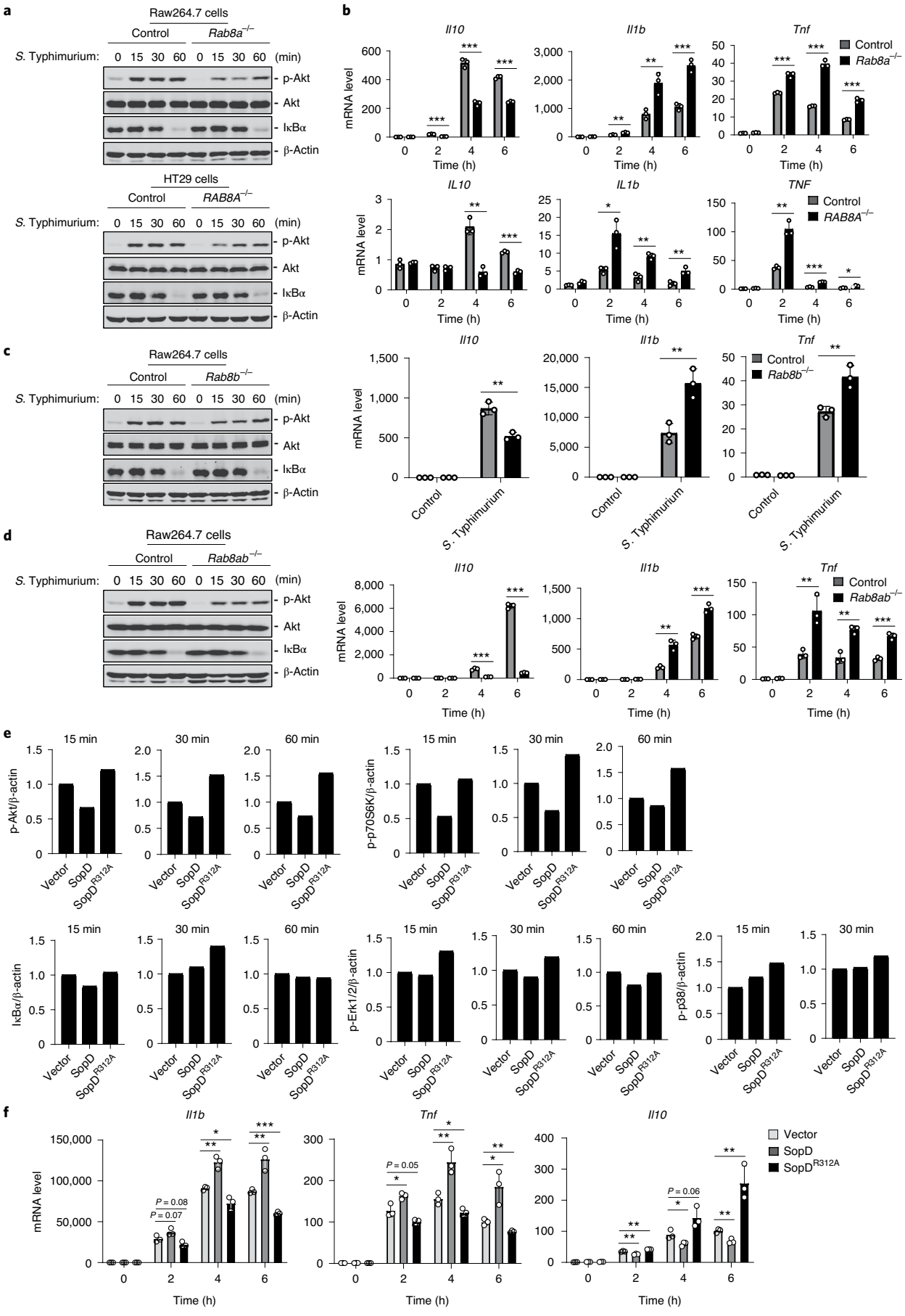
a
Raw264.7 cells
Control
Rab8a−/−
S. Typhimurium: 0 15 30 60 0 15 30 60 (min)
p-Akt
Akt
IκBα
β-Actin
HT29 cells
Control
RAB8A−/−
S. Typhimurium: 0 15 30 60 0 15 30 60 (min)
p-Akt
Akt
IκBα
β-Actin
b
Il10
Il1b
Tnf
mRNA level
Time (h)
Control
Rab8a−/−
IL10
IL1b
TNF
Control
RAB8A−/−
c
Raw264.7 cells
Control
Rab8b−/−
S. Typhimurium: 0 15 30 60 0 15 30 60 (min)
p-Akt
Akt
IκBα
β-Actin
Il10
Il1b
Tnf
mRNA level
Control
Rab8b−/−
Control
S. Typhimurium
d
Raw264.7 cells
Control
Rab8ab−/−
S. Typhimurium: 0 15 30 60 0 15 30 60 (min)
p-Akt
Akt
IκBα
β-Actin
Il10
Il1b
Tnf
mRNA level
Time (h)
Control
Rab8ab−/−
e
15 min
30 min
60 min
p-Akt/β-actin
p-p70S6K/β-actin
IκBα/β-actin
p-Erk1/2/β-actin
p-p38/β-actin
Vector
SopD
SopDR312A
f
Il1b
Tnf
Il10
mRNA level
Time (h)
P = 0.08
P = 0.07
P = 0.05
P = 0.06
Vector
SopD
SopDR312A

occur after SopD binding (Fig. 3d and Supplementary Fig. 8). These conformational changes position residues Thr 74, Arg 79, Tyr 5 and Lys 58 in Rab8 to engage in critical interactions with residues Gln 107, Tyr 278, Glu 240 and Glu 293 in SopD.

To examine the potential functional significance of the observed SopD–Rab8 interface, we introduced structurally guided mutations into SopD residues (Q107L/Q238L, S138A/Y278A and E293A) that are predicted to have a role in the formation of the complex. We then purified the resulting mutant proteins and examined their ability to form a complex with Rab8 in vitro. We found that the introduction of one of the mutations (E293A) completely abolished the ability of SopD to form a complex with Rab8 in vitro, demonstrating the importance of this interface in the formation of the SopD–Rab8 complex (Fig. 3e and Extended Data Fig. 7). Consistent with this finding, introducing the E293A mutation also disrupted the ability of SopD to interact with Rab8 in transient transfection experiments in cultured cells (Fig. 3f and Extended Data Fig. 8). Notably, critical SopD residues that are necessary for its interaction with Rab8 (such as Glu 293) are absent from SopD2 (Supplementary Fig. 1), which is consistent with the inability of SopD2 to form a complex with Rab8 (Extended Data Fig. 2). These results indicate that the identified interface is critical for the formation of the Rab8–SopD complex. We also examined the GAP activity of different SopD mutants, including the mutant (E293A) that disrupted its ability to form a complex with Rab8. We found that none of the mutations affected the GAP activity of this effector protein (Fig. 3g). Taken together, these results indicate that the interface captured in the SopD–Rab8 complex is unrelated to the GAP activity of SopD and suggest the presence of an additional function associated with this effector protein.

SopD activates Rab8 through a functional interface unrelated to its GAP activity. The molecular interface between SopD and Rab8 suggested the presence of a potential additional function in this effector protein independent of its GAP activity. To investigate this hypothesis, we examined the levels of Rab8 activation in HEK293T cells that had been transiently transfected with plasmids expressing wild-type SopD, its GAP catalytic mutant ($SopD^{R312A}$), a mutant that disrupts its interaction with Rab8 ($SopD^{E293A}$) or a mutant defective for both activities ($SopD^{R312A/E293A}$). Alternatively, we cotransfected the same plasmids along with a plasmid expressing rabin8, an exchange factor for Rab8 (ref. [35]). To assess the levels of Rab8 GTP loading, which is a measure of its activation, we took advantage of a previous observation that indicated that mical-L2, which is an effector of various Rab GTPases, can selectively bind to GTP-loaded Rab8 (ref. [36]). We found that the expression of wild-type SopD did not significantly alter the levels of GTP-loaded Rab8 in comparison to controls (Fig. 4a and Supplementary Fig. 9a). However, expression of $SopD^{R312A}$ resulted in an increased level of GTP-loaded Rab8, whereas expression of $SopD^{E293A}$ led to a reduction in the levels of activated Rab8 (Fig. 4a and Supplementary Fig. 9a). The observed effects were also apparent when the mutant proteins were coexpressed with rabin8 (Fig. 4b and Supplementary Fig. 9b). Expression of the SopD mutant defective in both activities ($SopD^{R312A/E293A}$) did not alter the levels of GTP-loaded Rab8 in comparison to controls (Fig. 4a,b and Supplementary Fig. 9a,b). Taken together, these results are consistent with the notion that, in addition to the negative regulatory GAP activity, SopD has Rab8 stimulatory activity that depends on the functional interface identified through the structural analysis.

The observation that SopD possesses a Rab8-activating function prompted us to investigate whether SopD exhibited guanine nucleotide exchange factor (GEF) activity. We detected no GEF activity in SopD, although, as predicted previously[35], we detected robust exchange activity of the Rab8 exchange factor rabin8 (Extended Data Fig. 9). SopD must therefore activate Rab8 through an alternative mechanism. After their activation and membrane targeting, small GTPases are extracted from the plasma membrane and maintained in a cytosolic soluble form by cognate regulatory proteins known as GDIs. These regulators have a critical role in the functional recycling of Rab GTPases[37,38]. After reception of an appropriate signal, the GDP-Rab GTPases must be released from their GDIs before their activation and membrane targeting[39–41]. We therefore examined whether SopD could displace Rab8 from its cognate GDI. In cultured HEK293T cells, we expressed epitope-tagged versions of Rab8 and GDI2 and examined their interaction using co-immunoprecipitation analysis in the presence of purified wild-type SopD, its GAP defective mutant ($SopD^{R312A}$) or a mutant that disrupts its interaction with Rab8 ($SopD^{E293A}$). We found that the addition of increasing amounts of purified wild-type SopD or its GAP-defective mutant ($SopD^{R312A}$) resulted in a significant reduction in the amount of Rab8 bound to GDI2 (Fig. 4c,d). By contrast, the addition of purified $SopD^{E293A}$ or SopD2, which are unable to form a complex with Rab8, did not affect the levels of Rab8 bound to GDI2 (Fig. 4d). We also expressed in HEK293T cells the same SopD mutants along with the epitope-tagged version of Rab8 and GDI2, and examined the levels of Rab8 bound to GDI2 using a co-immunoprecipitation assay. We found that the levels of Rab8 bound to GDI2 significantly decreased after expression of wild-type SopD or its GAP catalytic mutant ($SopD^{R312A}$) but remained unchanged when coexpressed with $SopD^{E293A}$ (Fig. 4e and Supplementary Fig. 9c). Taken together, these results indicate that SopD has the ability to stimulate Rab8 by promoting its dissociation from its cognate GDI.

Fig. 3 | Crystal structure of the SopD–Rab8 complex and functional analyses of the binding interface. a, Ribbon representation of the overall structure of the SopD–RAB8A complex. The secondary structure features of SopD, as well as the position of the switch I (grey), switch II (orange) and P-loop (light blue) regions of Rab8 are indicated. The key catalytic residue Arg 312 in SopD is shown as a stick and is highlighted in red. GDP is denoted as a stick (cyan), and water molecules and Mg^{2+} are represented as red and green spheres, respectively. Inset: the simulated annealing omit maps (yellow mesh) for GDP, water molecules and Mg^{2+} in the nucleotide-binding pocket of Rab8 from the SopD–RAB8A complex (contoured at 1.5σ). The Thr 22 residue of Rab8, which forms a coordinate bond with Mg^{2+}, is shown as a stick. Secondary structure elements are denoted. **b**,**c**, The interactions between SopD (green) and Rab8 (violet); interacting residues are shown as sticks. RabSF and RabF motifs are shown in yellow and light blue, respectively. Polar interactions are indicated by black dashes. The subscript r and s indicate the proteins Rab8 and SopD, respectively. **c**, Schematic of the interactions between Rab8 and SopD. The polar interactions are shown as blue dashed lines, the water (W) molecules as red balls and the hydrophobic interactions as black dashed lines. **d**, Structure superimposition of Rab8 as it appears in the Rab8–SopD complex, with Rab8 as it appears in complex with rabin8 or bound to GDP. Inset: the conformational changes of key amino acids in Rab8 after binding to SopD. **e**, Size-exclusion chromatography analyses of SopD carrying mutations in amino acids that define its interface with Rab8. The SDS-polyacrylamide gel electrophoresis analyses of the elution fractions is shown in Extended Data Fig. 7. **f**, Co-immunoprecipitation analyses of the interaction of SopD and its indicated mutants with Rab8 after transient expression in HEK293T cells. This experiment was conducted at least three times with equivalent results. **g**, GAP activity of the indicated SopD mutants with substitutions in amino acid residues that are involved in its interface with Rab8. Data are the mean ± s.d. ratio of GTPase activity observed in the presence or absence of SopD from three independent experiments. Statistical analysis was performed using one-way ANOVA with Dunnett's method; NS, not significant ($P > 0.05$); ***$P < 0.001$. $SopD^{FM}$, SopD lacking its first 34 amino acids encoding its TTS signal.

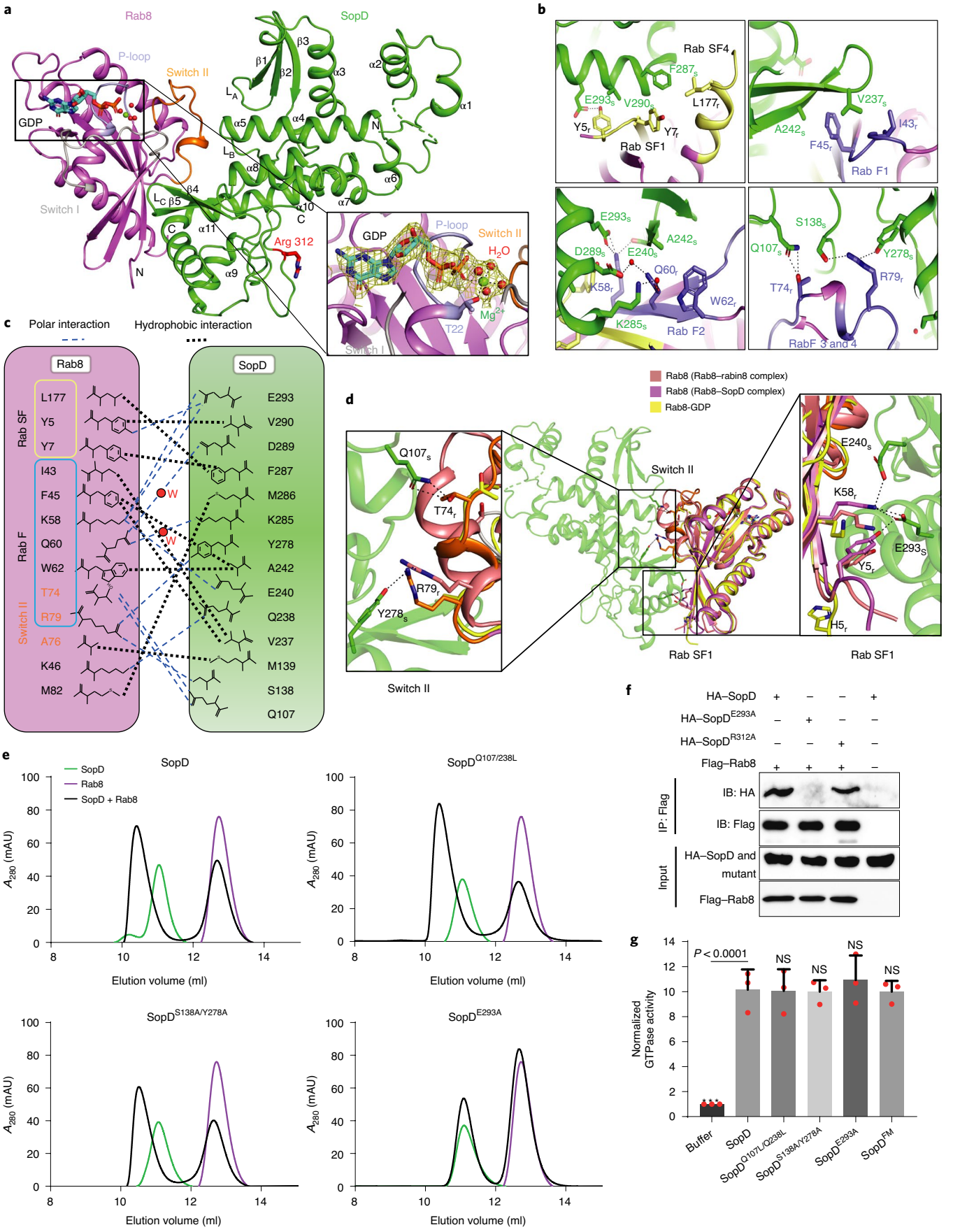
a
Rab8
SopD
P-loop
Switch II
GDP
Switch I
Arg 312
b
Rab SF4
Rab SF1
Rab F1
Rab F2
RabF 3 and 4
c
Polar interaction
Hydrophobic interaction
Rab8
SopD
Rab SF
Rab F
Switch II
d
Rab8 (Rab8–rabin8 complex)
Rab8 (Rab8–SopD complex)
Rab8-GDP
Switch II
Rab SF1
e
SopD
Rab8
SopD + Rab8
Elution volume (ml)
f
HA–SopD
HA–SopD^E293A
HA–SopD^R312A
Flag–Rab8
IP: Flag
IB: HA
IB: Flag
Input
HA–SopD and mutant
Flag–Rab8
g
P < 0.0001
NS
Normalized GTPase activity
Buffer
SopD
SopD^Q107L/Q238L
SopD^S138A/Y278A
SopD^E293A
SopD^FM

Mechanistic insight for the Rab8-activating function of SopD inferred from the crystal structure of the SopD–Rab8 complex. To gain insights into the potential mechanism by which SopD displaces GDI, we compared the atomic interface between SopD and Rab8 with the interface between the yeast Rab GTPase Ypt1 and its GDI (PDB: 2BCG). Comparison of the two structures shows that, although there is significant overlap between the two interfaces on the 'open end' of the V-shaped complex, this is not the case on the 'closed end' of the complex (Fig. 5a,b). At the closed end, there are no significant interactions between Ypt1 and its GDI but SopD engages Rab8 in unique interactions. These interactions include the SF (Tyr 5, Tyr 7 and Leu 177) and F2 regions (Lys 58 and Gln 60) of Rab8 as well as less conserved amino acid residues, such as Lys 46 and Met 82 (Fig. 5b). These interactions may provide the structural basis for the initial engagement of GDI-bound Rab8 by SopD, which would ultimately lead to conformational changes that destabilize the Rab8–GDI complex. In support of this notion, a mutation of a critical residue in SopD—SopD^{E293A}, which specifically interacts with Tyr 5 and Lys 58 in Rab8—effectively prevented the ability of SopD to displace GDI from Rab8 (Fig. 4d,e). We propose that the initial engagement of the close end of the Rab8–GDI complex by SopD leads to the destabilization of critical Rab8–GDI interactions that maintain the stability of the complex, exemplified by a network of hydrogen bonds between Asp 44 in Ypt1, and Arg 106, Tyr 107, Arg 248 and Arg 445 in the GDI (Fig. 5c). The SopD-induced destabilization of this network would lead to an outward movement of ~4 Å of the GDI-binding platform (centred on the Gly 42 residue in the case of Ypt1). These conformational changes would also lead to repulsive interactions between Ile 252 in the GDI and Gly 42 and Asp 44 in Rab8 (Fig. 5c). Furthermore, the switch-II region of Ypt1, which interacts strongly with GDI, would be also disrupted by SopD binding (Fig. 5d). These conformational changes would result in a ~6 Å inward movement of switch II, therefore destabilizing critical hydrophobic interactions between this region (such as residue Ala 65 in Rab8) and a hydrophobic patch in GDI formed by Ala 247, Ala 251 and Ile 252 (Fig. 5d). The SopD-induced conformational changes in switch II would also destabilize additional critical Rab8–GDI interactions exemplified by those between residues Thr 72 and Ser 75 in Ypt1 (or the corresponding Thr 72 and Thr 75 residues in Rab8) and Tyr 44 and Gln 244 in GDI (Fig. 5d). In summary, we propose a model whereby, by engaging Rab8 residues that are not involved in its interaction with GDI, SopD triggers conformational changes in critical regions of Rab8, in particular switch II, resulting in the destabilization of the Rab8–GDI complex and the subsequent release of GDI.

SopD positively and negatively modulates *S.* Typhimurium-induced inflammatory signalling through its independent Rab8-modulating activities. The discovery that SopD has the ability to both activate and inhibit Rab8 prompted us to investigate the potential role of these activities in the context of *Salmonella* infection. We infected Raw264.7 macrophages and HT29 intestinal epithelial cells with wild-type *S.* Typhimurium or its isogenic mutants Δ*sopD*, *sopD*^{R312A} or *sopD*^{E293A}. To facilitate interpretation of the results, we also introduced a Δ*sopD2* deletion, as this effector protein also exhibits Rab8 GAP activity, although it lacks Rab8-activating activity (as described above). We found that infection of either cell line with *S.* Typhimurium expressing the GAP-defective SopD^{R312A} mutant resulted in significantly higher Akt activation compared with cells infected with the wild type (Fig. 6a and Supplementary Fig. 10). By contrast, cells infected with *S.* Typhimurium expressing SopD^{E293A}, which is defective for Rab8 activation, resulted in a decrease in Akt activation (Fig. 6a and Supplementary Fig. 10). Consistent with these observations, cells infected with the *S.* Typhimurium Δ*sopD2 sopD*^{R312A} mutant showed increased levels of the anti-inflammatory cytokine IL-10 and decreased levels of the pro-inflammatory cytokines IL-1β and TNFα (Fig. 6b and Extended Data Fig. 10). By contrast, cells infected with *S.* Typhimurium expressing the *sopD*^{E293A} allele showed the reversed pattern—decreased levels of IL-10 and increased levels of IL-1β and Tnfα (Fig. 6b and Extended Data Fig. 10). This is consistent with the notion that SopD has the ability to both enhance and suppress the inflammatory response to *S.* Typhimurium during infection.

We also compared the intestinal inflammatory response of mice infected with *S.* Typhimurium Δ*sopD2* strains expressing either the SopD^{R312A} GAP-deficient mutant or the SopD^{E293A} mutant, which is deficient for Rab8 activation. We found significantly lower levels of mRNA encoding the pro-inflammatory cytokines IL-1β and TNFα in the intestines of mice infected with the *S.* Typhimurium strain expressing the *sopD*^{R312A} GAP-deficient allele compared with mice expressing wild-type SopD (Fig. 6c). The difference was more pronounced when compared with the levels found in the intestines of mice infected with the *S.* Typhimurium strain expressing the SopD^{E293A} mutant that is deficient for Rab8 activation, which showed increased levels of pro-inflammatory cytokine mRNA even when compared with mice infected with the wild type (Fig. 6c). Taken together, these results indicate that, through its contrasting Rab8-modulating activities, the effector protein SopD has the ability to enhance and suppress the inflammatory response to *S.* Typhimurium.

Discussion

Here we described a *S.* Typhimurium TTSS effector protein that can stimulate both pro- and anti-inflammatory signalling. This bifunctional effector accomplishes this feat by targeting an anti-inflammatory pathway orchestrated by the Rab8 GTPase[15–17]. Through agonistic and antagonistic activities towards Rab8, SopD can alternatively suppress or enhance the inflammatory response to *Salmonella* (Fig. 6d).

Rab8 is linked to anti-inflammatory signalling emanating from TLR4 (refs. [15–17]). As *Salmonella* LPS is a potent activator

Fig. 4 | SopD activates Rab8 through a functional interface unrelated to its GAP activity. a,**b**, The effect of the transient expression of SopD^{R312A} (a GAP-defective mutant) or SopD^{E293A} (a mutant that is unable to form a complex with Rab8) on the levels of Rab8 activation. HEK293T cells were transiently co-transfected with plasmids expressing wild-type SopD or the indicated mutants along with plasmids expressing GFP-tagged RAB8A (**a**) and, when indicated, Flag-tagged rabin8 (**b**), an exchange factor for RAB8A. Twenty hours after transfection, cells were lysed and the levels of GTP-loaded Rab8A were determined using the GST-Mical-L2 affinity probe (Methods). The quantification of the western blots is shown in the accompanying graphs. Values are represented relative to those obtained with the vector control, which was given an arbitrary value of 1. A repetition of this experiment is shown in Supplementary Fig. 9. **c**–**e**, SopD displaces GDI2 from RAB8A. HEK293T cells were cotransfected with plasmids expressing HA-tagged GDI2 and Flag-tagged Rab8. Then, 24 h after transfection, cells were lysed, and 0.1 μg ml^{-1}, 0.5 μg ml^{-1} or 1 μg ml^{-1} of purified SopD (**c**), or 1 μg ml^{-1} of purified SopD, SopD^{R312A}, SopD^{E293A} or SopD2 (**d**) was added to the cell lysates, and the levels of RAB8A–GDI2 complex were determined using immunoprecipitation with anti-Flag antibodies (directed to the tag in RAB8A) and immunoblotting with anti-HA antibodies (directed to the tag in GDI2). **e**, Alternatively, HEK293T cells were transiently cotransfected with plasmids expressing GFP-tagged RAB8A and Flag-tagged GDI2, along with plasmids expressing the indicated HA-tagged SopD constructs. Twenty hours after transfection, cells were lysed and the levels of RAB8A–GDI2 complex were determined using immunoprecipitation with anti-Flag antibodies (directed to the tag in GDI2) and immunoblotting with anti-GFP antibodies (directed to the tag in RAB8A). The quantification of the western blots is shown in the accompanying graph. Values are represented relative to those obtained with vector control, which was given an arbitrary value of 1. A repetition of this experiment is shown in Supplementary Fig. 9.

of TLR4, it is possible that SopD exerts its effect in the context of LPS-mediated signalling. However, we have also shown that *S.* Typhimurium can trigger SPI-TTSS- and Rab8-dependent Akt-mediated anti-inflammatory signalling in cultured intestinal epithelial cells that do not respond to LPS. These findings therefore indicate that, by inhibiting Rab8 through its GAP

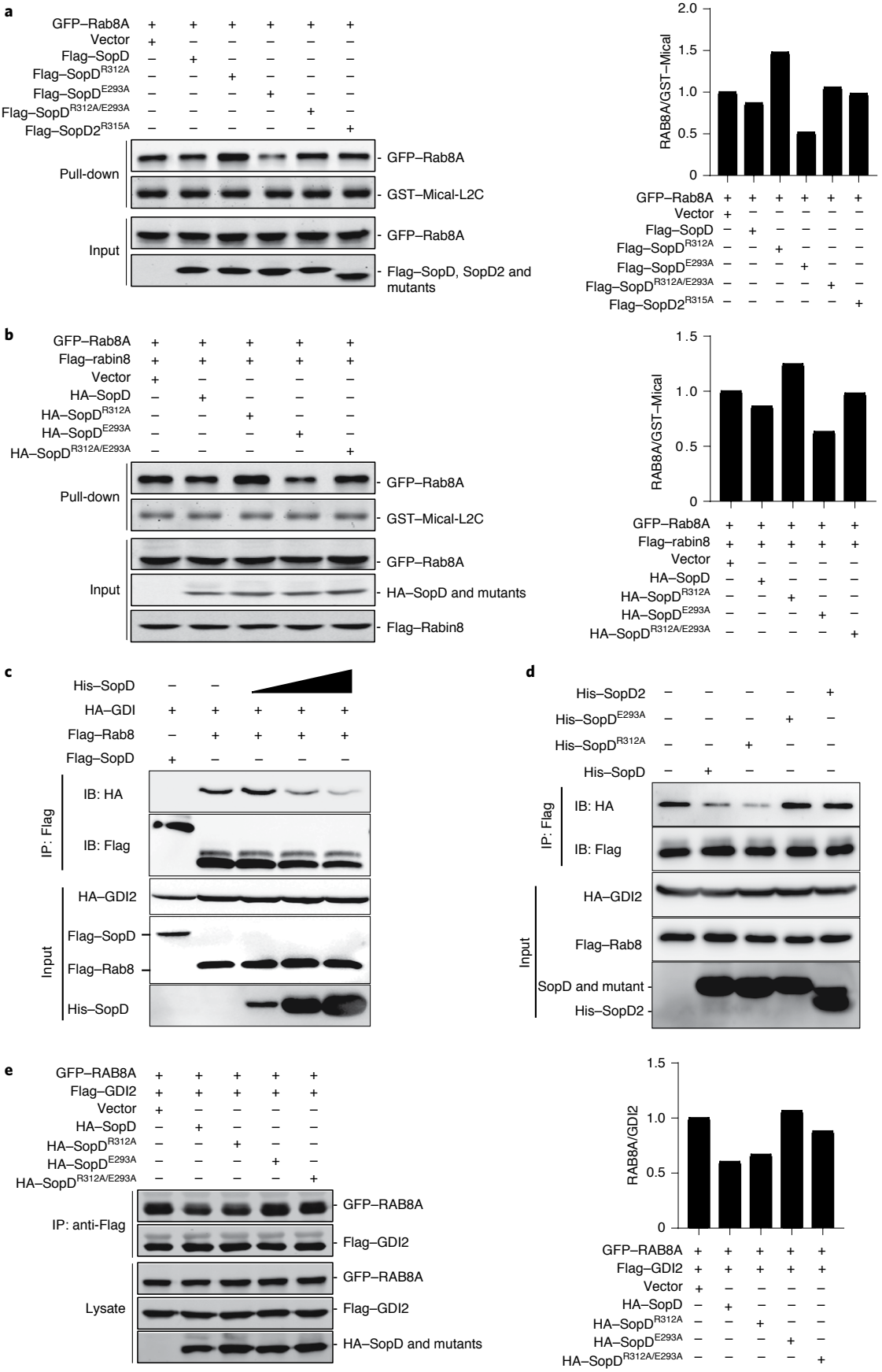

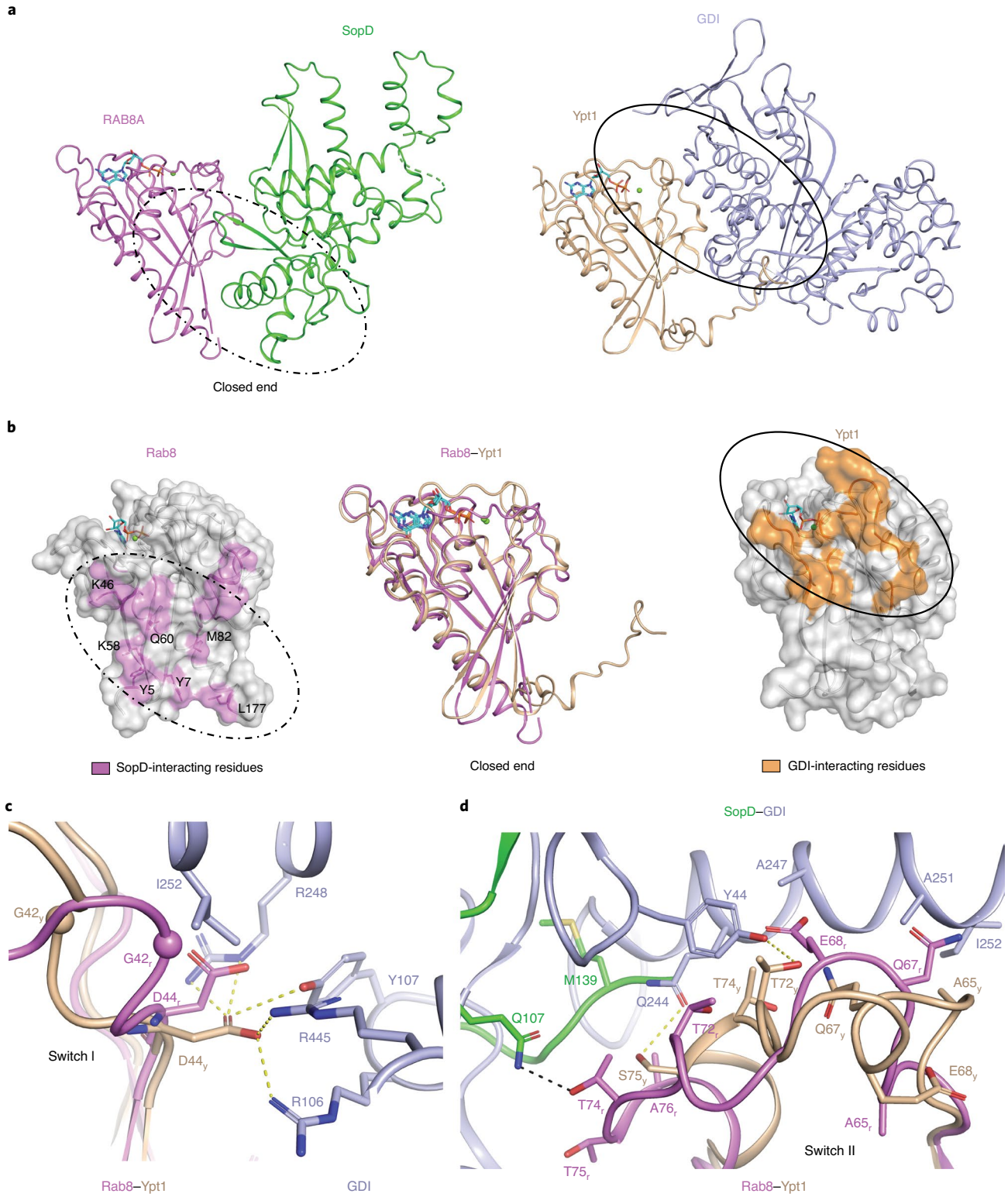

Fig. 5 | The structural basis for GDI displacement by SopD. a, Ribbon representation of the overall structure of the SopD–RAB8A and Ypt1–GDI (PDB: 2BCG) complexes. **b**, SopD and GDI bind to different surfaces on their cognate Rab GTPases. The residues of Rab8 and Ypt1 involved in their intermolecular interactions with SopD and GDI, respectively, are shown on their surface structures in pink and orange, respectively (left and right). The structural alignment between Rab8 from the SopD–Rab8 complex structure and Ypt1 from the GDI–Ypt1 complex are shown as a ribbon (middle). The Rab8 amino acid residues that are specifically involved in its interaction with SopD at the closed end of the Rab8–SopD complex are shown as sticks. In **a** and **b**, GDP and Mg^{2+} bound to Rab8 or Ypt1 are represented as sticks and spheres, respectively. The interfaces between SopD and Rab8, and between GDI and Ypt1 are highlighted with dotted and solid line circles, respectively. **c**,**d**, SopD-induced conformational changes in switch I (**c**) and switch II (**d**) of Rab8, highlighting the residues that are involved in GDI binding. Key interacting residues in Rab8 ($G42_{Rab8}$) and Ypt1 ($G42_{Ypt1}$) are shown as a ball representation. Other SopD-interacting residues involved in the GDI displacement process are shown as sticks. Hydrophobic interactions between Ypt1 and Rab8, and between GDI and SopD are denoted by yellow and black dashed lines, respectively. The subscript r and y indicate the proteins Rab8 and Ypt1, respectively.

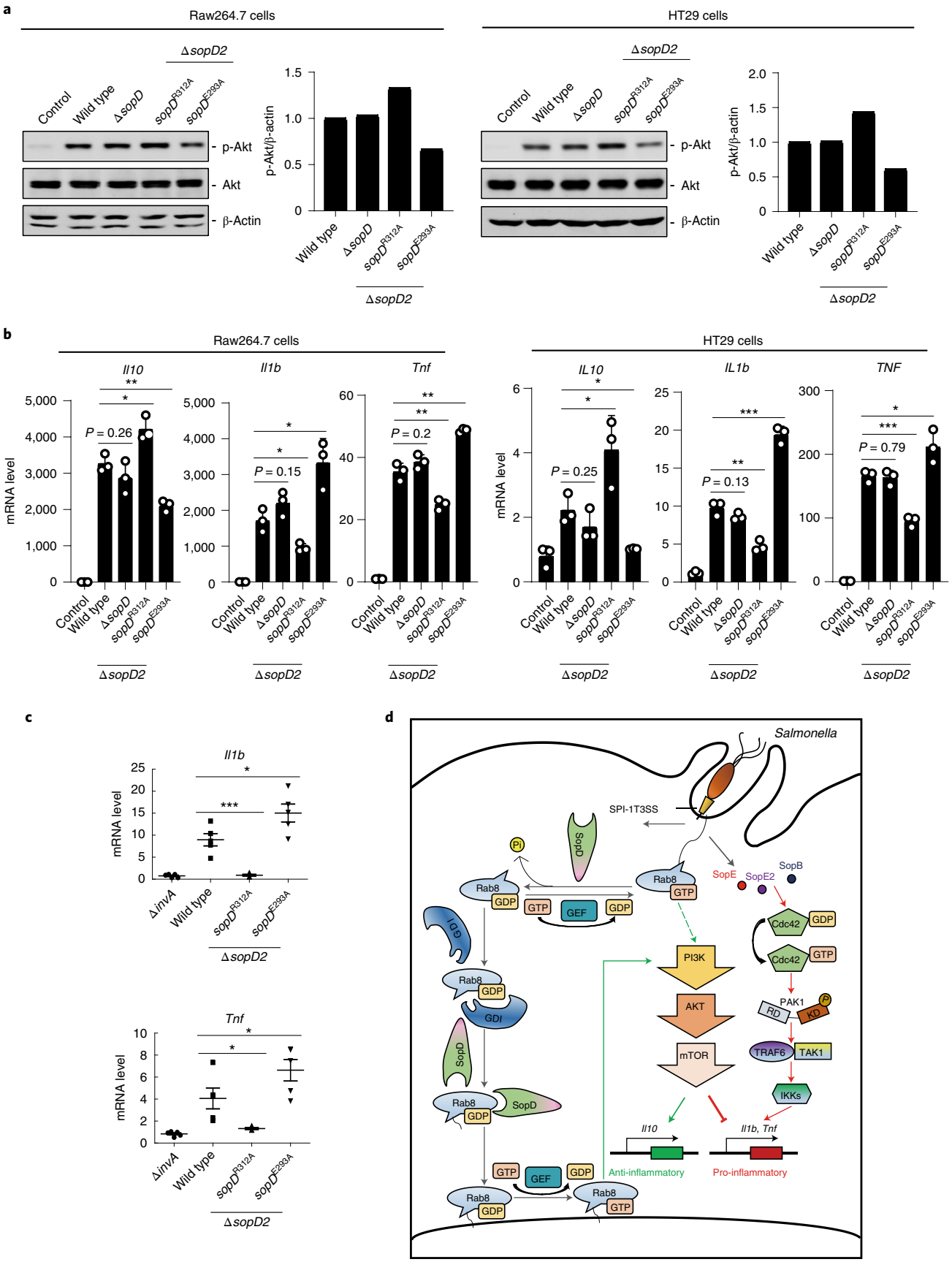

activity, SopD can exert its pro-inflammatory effect in the context of both LPS and *Salmonella*-induced anti-inflammatory signalling.

We have also shown that SopD can stimulate Rab8-dependent anti-inflammatory signalling by displacing Rab8 from its cognate GDI. Through structure and function analyses, we have shown that

Fig. 6 | SopD positively and negatively modulates *S.* Typhimurium-induced inflammatory signalling through its independent Rab8-modulating activities. **a**,**b**, Akt activation and cytokine gene expression in cells infected with *S.* Typhimurium strains expressing different *sopD* mutants. **a**, Raw264.7 (m.o.i. = 2) or HT29 (m.o.i. = 10) cells were infected with wild-type *S.* Typhimurium, the Δ*sopD* isogenic mutant or the Δ*sopD2* mutant expressing the indicated mutant alleles of *sopD* for 60 min. Akt activation was analysed using immunoblotting with antibodies specific for phosphorylated Akt and β-actin (as a loading control). The quantification of the western blots is shown in the adjacent graphs. Values are represented relative to those obtained with the wild type, which was given an arbitrary value of 1. A repetition of this experiment is shown in Supplementary Fig. 10. **b**, Alternatively, Raw264.7 (m.o.i. = 5) or HT29 (m.o.i. = 20) cells were infected with the same *S.* Typhimurium strains (as indicated) and, 4 h after infection, the mRNA levels of the indicated cytokines were quantified using qPCR. Data are mean ± s.d. fold induction relative to uninfected controls of three independent determinations. Statistical analysis was performed using unpaired two-sided *t*-tests; $*P < 0.05$, $**P < 0.01$, $***P < 0.001$; NS, not significant ($P > 0.05$). **c**, C57BL/6 *Slc11a1*$^{+/+}$ (also known as *Nramp1*) mice ($n = 5$ animals per strain) were orally infected (~1×10^8 colony-forming units) with wild-type *S.* Typhimurium, its isogenic Δ*invA* (TSS defective) mutant (as a negative control) or the *S.* Typhimurium Δ*sopD2* strains expressing the *sopD*^{R312A} or *sopD*^{E293A} alleles. Then, 4 d after infection, the transcription levels of the indicated cytokine genes in the cells of the intestinal caeca were analysed using qPCR. Data are mean ± s.d. fold induction relative to animals infected with the *S.* Typhimurium Δ*invA* mutant strain. Statistical analysis was performed using unpaired two-sided *t*-tests; $*P < 0.05$, $***P < 0.001$. **d**, The model for SopD action during *Salmonella* infection. *Salmonella* delivers TTSS effector proteins that activate membrane ruffling, inflammatory signalling, and the activation and recruitment Rab8 to the membrane ruffles. The GAP activity of SopD reverses the activation of Rab8, therefore delaying or preventing Akt-dependent anti-inflammatory signalling. Later during infection, SopD stimulates Rab8 through its GDI-displacement activity, leading to the stimulation of the anti-inflammatory program.

the function of SopD resembles that of eukaryotic GDI displacement factors, which release Rab GTPases from their GDIs, therefore enabling their recycling to the plasma membrane where they can be activated by their cognate GEFs[40,41].

The opposing activities of SopD raise the question of how these activities are coordinated in time (Fig. 6d). As pro-inflammatory signalling precedes the anti-inflammatory response, it follows that the GAP activity of SopD should precede its Rab8 stimulatory activity. In fact, TTSS-mediated pro-inflammatory signalling occurs immediately after infection; it would therefore be expected that the SopD pro-inflammatory activity through its GAP enzymatic function should be exerted very early during infection, along with that of the Cdc42 agonists SopE, SopE2 and SopB. The cell homeostasis recovery process would then be initiated by the Rab8-agonist activity of SopD, along with the activities of other TTSS effectors, such as SptP, which antagonizes Cdc42 (ref. [11]); SopB, which activates Akt[29]; as well PipA, GogA and GtgA, which directly target the NF-κB transcription factors for degradation[12]. In all cases, substrate availability (that is, GTP-loaded or GDI-bound Rab8) ultimately defines which of the SopD activities are exerted at a given time during infection.

In summary, here we have described a bifunctional bacterial effector protein that can exert agonistic and antagonistic activity towards a single target, Rab8, and therefore modulate the inflammatory response. This is a remarkable example of a bacterial determinant shaped by long-standing host–pathogen interactions aimed at facilitating pathogen replication while preserving host homeostasis.

Methods

Bacterial strains. A list of all of the *S.* Typhimurium strains described is provided in Supplementary Table 1; the strains were derived from the wild-type isolate SL1344 (ref. [42]), and were constructed using standard recombinant DNA and allelic exchange procedures as previously described[43] using the *E. coli* β-2163 Δ*nic35* as the conjugative donor strain[44]. Strains were routinely cultured in lysogeny broth (LB) broth at 37 °C.

Cell lines. HEK293T, HT29 and Raw264.7 cells were obtained from ATCC. Cells were cultured in Dulbecco's modified Eagle medium (DMEM, GIBCO) supplemented with 10% fetal bovine serum at 37 °C with 5% CO_2 in a humidified incubator. All of the cell lines were routinely tested for mycoplasma contamination using a Mycoplasma Detection Kit (Southern Biotech, 13100-01).

Plasmid construction. For recombinant protein expression in *E. coli*, the full-length *sopD*, *sopD2* and the truncated *sopD*$^{34–end}$, lacking its TSS signal, were cloned into the pET15b expression vector with an N-terminal His tag. Full-length *RAB8A* and truncated *RAB8A*$^{1–183}$ were cloned into the pET15b vector (Novagen), introducing an N-terminal 6-His tag, or into the pET28a vector, introducing an N-terminal 6×His-SUMO (small ubiquitin-like motif) tag. Expression vectors for all of the other human Rab GTPases used in this study were constructed by cloning the different Rab GTPases into the pET15b vector. For expression in mammalian cells, the *sopD* and *sopD2* genes were amplified from *S.* Typhimurium SL1344 and cloned into the pRK-5 or pSin3xHA vectors to generate N-terminal FLAG- or HA-tagged versions of these proteins, respectively. The *RAB8A* gene was cloned into the pRK-5 vector introducing an N-terminal Flag or GFP tag. The *GDI2* cDNA was amplified from cDNA obtained from HEK293T cells using reverse transcription, or from a plasmid encoding this gene (pCellFree_G03 GDI2, Addgene) and cloned into pRK-5, resulting in N-terminal HA- or FLAG-tagged versions of this protein. A cDNA encoding rabin8$^{153–237}$ was amplified from HEK293T cells and cloned into the pET28a vector with an N-terminal 6×His-SUMO tag or from a plasmid encoding full-length rabin8 (Flag–rabin8, Addgene). All truncations and point mutations were generated using the Gibson assembly strategy[45]. All plasmids were verified by DNA sequencing.

Protein expression and purification. *E. coli* B21 (DE3) carrying plasmids expressing the different His-tagged SopD constructs were grown in LB medium to an optical density at 600 nm (OD_{600}) of 0.8, expression of the different proteins was induced by addition of 0.4 mM isopropyl-*β*-D-thiogalactopyranoside and cultures were further incubated for 12 h at 25 °C. Bacterial cells were collected by centrifugation and the pellets were resuspended in lysis buffer (20 mM Tris-HCl (pH 8.0), 150 mM NaCl). Bacterial cells were lysed using a high-pressure cell crusher (Union-Biotech), the supernatants were collected, run through a Ni-NTA agarose resin (Qiagen), washed with 20 mM Tris-HCl (pH 8.0), 150 mM NaCl and 20 mM imidazole, and proteins were eluted in the same buffer with 300 mM imidazole. Proteins were further purified using HiTrap Q HP ion-exchange and Superdex 200 Increase 10/300 GL (GE Healthcare Life Sciences) chromatography. Full-length His-tagged Rab8a and truncated Rab8a$^{1–183}$ were expressed in *E. coli* BL21(DE3) grown in Terrific broth at 25 °C for 48 h. The different Rab proteins were purified using Ni-NTA agarose resin (Qiagen) as described previously[19], the SUMO tag was removed with homemade His-tagged ULPI protease at room temperature for 2 h and proteins were further purified using Superdex 200 gel-filtration chromatography.

To prepare SopD (or its mutants) in complex with RAB8A, purified His–SopD (or its mutants) was incubated with Rab8a$^{1–183}$ at a molar ratio of 1:3 at room temperature for 2 h in a buffer containing 20 mM Tris (pH 7.5), 150 mM NaCl, 2 mM $MgCl_2$, 1 μm GTPγS (or 20 mM NaF, 0.2 mM $AlCl_3$ and 1 μm GDP) and 3 mM dithiothreitol. The stable complex was obtained after Superdex 75 Increase 10/300 GL or Superdex 200 Increase 10/300 GL column chromatography. As negative controls, the respective monomers were analysed using gel-filtration chromatography in an identical manner.

Protein crystallization and structure determination. The crystals of the SopD–Rab8 complex were grown at 18 °C using the hanging-drop vapour diffusion method by mixing the protein and well solution at a 1:1 ratio. Crystals were obtained under 0.05 M sodium cacodylate trihydrate (pH 6.5), 0.2 M $MgCl_2$ and 11.5% PEG 4000. The crystals of the SopD–Rab8 complex were soaked with 30% glycerol then flash-cooled in liquid nitrogen. Diffraction data were collected on the BL17U1 beamline at the Shanghai Synchrotron Radiation Facility and processed using the XDS package[46]. The phase of this structure was determined by molecular replacement using SopD (PDB: 5CPC) and Rab8 (PDB: 4LHW) structures as searching models and the Phaser program in CCP4 (ref. [47]). The model was manually built with Coot[48]. All of the structures were refined with PHENIX[49], and manual modelling was performed between refinement cycles. Statistics of data collection and refinement are summarized in Supplementary Table 2. All of the structures were prepared for graphic display using PyMOL[50].

Co-immunoprecipitation and immunoblotting analyses. HEK293T cells were transiently transfected with plasmid DNA encoding the indicated proteins or empty vector (as indicated in the figure legends) using the Lipofectamine 2000 reagent (Invitrogen) according to the manufacturer's instructions. Then, 24 h or 48 h after transfection, ~1×10^7 cells were collected and lysed in 1 ml lysis buffer (20 mM Tris-HCl (pH 7.4), 150 mM NaCl, 1 mM EDTA and 1% NP-40) for 15 min on ice. The cell lysates were centrifuged at 14,000 r.p.m. for 15 min at 4 °C, supernatants were collected, mixed with anti-Flag M2 agarose affinity gel (Sigma-Aldrich), incubated for 3 h at 4 °C and beads were washed four times with cell lysis buffer containing 0.5 M NaCl. Protein bound to the resin was eluted by adding 3× Flag peptide (200 ng μl^{-1}) (MedChem Express) for 30 min at 4 °C and the eluates were analysed using western blotting. Alternatively, the beads were mixed with sample buffer before their separation on 10% SDS–PAGE. Proteins were transferred onto polyvinylidene fluoride (Millipore) or nitrocellulose membranes and processed for immunoblot analyses with the different antibodies as indicated in the figure legends. Blots were treated with the indicated primary antibodies (as indicated in the figure legends) and with either HRP-coupled or DyLight-conjugated secondary antibodies (emission 800 nm; Thermo Fisher Scientific). Blots were finally developed with M5 Hiper ECL Western HRP Substrate (Mei5 Biotechnology) or visualized using a LI-COR Odyssey imaging system. When required, the intensity of the bands was quantified with using Odyssey v.3.0 (LI-COR).

For competition binding assays, different concentrations of SopD or its mutants were added to the indicated cell lysates before the addition of the anti-Flag M2 agarose affinity gel, and samples were processed for co-immunoprecipitation as described above.

GAP assay. The intrinsic and GAP-accelerated GTP hydrolysis of the different GTPases was measured using the high throughput colorimetric GTPase assay kit (Innova Biosciences). In brief, purified Rab GTPases (15 μM) were mixed with the different SopD preparations (1.5 μM) in a buffer containing 50 mM Tris-HCl (pH 7.5), 150 mM NaCl, 2.5 mM $MgCl_2$ and 0.5 mM GTP. The mixture was dispensed onto 96-well microplates and incubated for 2 h at room temperature. The release of inorganic phosphate was quantified by measuring the absorbance at 635 nm of the different samples on a microplate reader (Tecan).

GEF assay. The GEF activity of SopD towards Rab8a was measured as previously described[51]. In brief, RAB8A was loaded with MANT-GDP by incubation with a twentyfold molar excess of MANT-GDP over the GTPase and a tenfold molar excess of EDTA over $MgCl_2$ for 1.5 h at room temperature. GDP binding was stabilized by adding $MgCl_2$ to twice the EDTA concentration. The buffer was subsequently exchanged with 20 mM Tris-HCl (pH 7.5), 150 mM NaCl and 2 mM $MgCl_2$ by gel-filtration chromatography. Mant-GDP-bound $Rab8a^{1-183}$ (2 μM) was incubated with 0.4 μM of $rabin8^{153-237}$ proteins (or 2 μM SopD, $SopD^{R312A,}$ $SopD^{E293A}$) in the presence of 5 μM of GTPγS in the reaction buffer (20 mM Tris-HCl (pH 7.5), 150 mM NaCl and 2 mM $MgCl_2$). Fluorescence of MANT-GDP was excited directly at 360 nm and detected at 450 nm. Fluorescence emission was read out every 10 s for a total of 1,200 s.

Rab8 activation assay. The levels of GTP-loaded Rab8, a measure of its activation, were determined using a previously developed assay on the basis of the ability of Mical-L2, which is an effector of various Rab GTPases, to selectively bind to GTP-loaded Rab8 (ref. [36]). GST–Mical-L2 was purified by affinity chromatography using glutathione Sepharose 4B beads according to the standard procedures. Plasmids encoding GFP-tagged RAB8A, Flag-tagged rabin8, along with HA- or Flag-tagged SopD or its mutants were co-transfected into HEK293T cells. Then, 24 h after transfection, cells were lysed in lysis buffer (20 mM Tris-HCl (pH 7.4), 150 mM NaCl, 1 mM EDTA, 1% NP-40) for 15 min on ice. The cell lysates were centrifuged at 14,000 r.p.m. for 15 min at 4 °C, and supernatants were collected and incubated with 1 μg of GST-tagged C-terminal fragment Mical-L2 for 1 h at 4 °C. The beads were then washed with lysis buffer, and the samples were analysed by immunoblotting with the appropriate antibodies.

***S.* Typhimurium cell infection.** *S.* Typhimurium was grown overnight in LB, cultures were diluted 1/20 into fresh LB containing 0.3 M NaCl and further grown to an OD_{600} of 0.9. Raw264.7 or HT29 cells were then infected with the indicated *S.* Typhimurium strains at the m.o.i. values indicated in the figure legends. Cells were then washed three times with Hank's balanced salt solution and treated with gentamicin (100 μg ml^{-1}) for 1 h to kill extracellular bacteria. Cells were then washed and cultured in medium with a low concentration of gentamicin (10 μg ml^{-1}) for the times indicated in the figure legends.

***S.* Typhimurium cell invasion assay.** The ability of *S.* Typhimurium to invade cultured cells was measured by the gentamicin protection assay as previously described[52].

Generation of CRISPR–Cas9-edited cell lines. Generation of CRISPR–Cas9-edited cell lines was carried out as described previously[53] according to standard protocols[54]. In brief, double-stranded oligonucleotides corresponding to the target sequences were cloned into the lenti-CRISPR-V2 vector and cotransfected with the packaging plasmids into HEK293T cells. Then, 2 d after transfection, the viruses were collected and used to infect Raw264.7 or HT29 cells. The virally transduced cells were selected in culture medium containing puromycin for 5 d, and the isolated clones were screened using PCR and sequencing to identify knockout cells. A list of the nucleotide sequence of the guide RNAs and primers used to construct the different cell lines is provided in Supplementary Table 3.

Generation of stable cell lines. Stable Raw264.7 cells expressing HA-tagged SopD or its different mutants were generated through viral transduction and puromycin selection. In brief, transducing viruses were produced by cotransfecting plasmids encoding HA-tagged SopD or its mutants along with the packaging plasmids into HEK293T cells. Then, 2 d after transfection, the viruses were collected and used to infect Raw264.7 cells. The infected cells were selected with puromycin for at least 5 d and resistant cells were tested for the expression of SopD or its mutants.

qPCR. qPCR of mRNA in cultured cells and mouse tissues was performed as described previously[12]. In brief, caeca from infected animals were removed, cut open, washed extensively with PBS and epithelial cells were collected into a centrifuge tubes by scraping the tissue with a glass slide. Total RNA from cultured cells or mouse caeca were isolated using TRIzol reagent (Invitrogen) according to the manufacture's protocol, and was reversed-transcribed with iScript reverse transcriptase (Bio-Rad). qPCR was performed using iTaq SYBR Green Supermix (Bio-Rad) in an iCycler real time PCR machine (Bio-Rad). Data shown are the relative abundance of the indicated mRNA normalized to that of *GAPDH*. A list of the primers used for the qPCR is provided in Supplementary Table 4.

Cytokine quantification. Raw264.7 cells were infected with different bacterial strains as indicated in the figure legends for 18 h. The levels of the cytokines IL-10, IL-1β and TNFα in the culture medium of infected cells were measured using an enzyme-linked immunosorbent assay as indicated by the manufacturer (BioLegend, 431417, 432604 and 430907, respectively). The actual concentration of the cytokines was determined using a standard curve (concentration range for the standards: IL-10 and TNFα: 15.6–1,000 pg ml^{-1}; IL-1β: 31.3–2,000 pg ml^{-1}).

Mouse infections. All of the animal experiments were conducted according to protocols approved by Yale University's Institutional Animal Care and Use Committee (IACUC) under protocol number 2019-07858. C57BL/6 male and female mice (aged 8 to 12 weeks) carrying a wild-type allele of *Slc11a1* (*Nramp1*)[55] were orally infected by stomach gavage with the different *S.* Typhimurium strains as previously described previously[12]. Then, 4 d after infection, mice were euthanized, and caeca were removed and processed for qPCR analysis as described above. The number of animals was determined on the basis of previous experience conducting similar experiments and the experimenter was not blinded to the different conditions. Animals were housed in a specific pathogen free animal facility at Yale University at an ambient 21–22 °C temperature room under a standard 12 h–12 h light–dark cycle (lights on 07:00–19:00) with chow and water provided ad libitum.

Statistical analysis. Experiments were performed at least three times independently. Data are shown as arithmetic mean ± s.d. unless otherwise stated. All statistical data were calculated using GraphPad Prism v.8.0 (GraphPad). For comparisons of the means of two groups, unpaired two-sided *t*-tests were used. For comparisons of multiple groups with a control group, one-way ANOVA was used; two-way ANOVA was used for multiple comparisons. The significance of mean comparison was annotated as follows: not significant; $^*P < 0.05$, $^{**}P < 0.01$, $^{***}P < 0.001$. $P < 0.05$ was considered to be statistically significant.

Reporting Summary. Further information on research design is available in the Nature Research Reporting Summary linked to this article.

Data availability

The atomic coordinates and structure factors generated in this study have been deposited in the PDB under the accession code 7BWT. Source data are provided with this paper.

Received: 25 June 2020; Accepted: 11 January 2021;
Published online: 18 February 2021

References

1. Chen, L. M., Hobbie, S. & Galan, J. E. Requirement of CDC42 for *Salmonella*-induced cytoskeletal and nuclear responses. *Science* **274**, 2115–2118 (1996).
2. Bruno, V. M. et al. *Salmonella* Typhimurium type III secretion effectors stimulate innate immune responses in cultured epithelial cells. *PLoS Pathog.* **5**, e1000538 (2009).
3. Patel, J. C. & Galan, J. E. Differential activation and function of Rho GTPases during *Salmonella*-host cell interactions. *J. Cell Biol.* **175**, 453–463 (2006).

4. Sun, H., Kamanova, J., Lara-Tejero, M. & Galán, J. E. *Salmonella* stimulates pro-inflammatory signalling through p21-activated kinases bypassing innate immune receptors. *Nat. Microbiol.* **3**, 1122–1130 (2018).
5. Hobbie, S., Chen, L. M., Davis, R. & Galán, J. E. Involvement of the mitogen-activated protein kinase pathways in the nuclear responses and cytokine production induced by *Salmonella* Typhimurium in cultured intestinal cells. *J. Immunol.* **159**, 5550–5559 (1997).
6. Kamanova, J., Sun, H., Lara-Tejero, M. & Galán, J. The *Salmonella* effector protein SopA modulates innate immune responses by targeting TRIM E3 ligase family members. *PLoS Pathog.* **12**, e1005552 (2016).
7. Keestra, A. et al. A *Salmonella* virulence factor activates the NOD1/NOD2 signaling pathway. *mBio* **2**, e00266-11 (2011).
8. Haraga, A. & Miller, S. I. A *Salmonella* type III secretion effector interacts with the mammalian serine/threonine protein kinase PKN1. *Cell Microbiol.* **8**, 837–846 (2006).
9. Stecher, B. et al. *Salmonella enterica* serovar Typhimurium exploits inflammation to compete with the intestinal microbiota. *PLoS Biol.* **5**, 2177–2189 (2007).
10. Winter, S. et al. Gut inflammation provides a respiratory electron acceptor for *Salmonella*. *Nature* **467**, 426–429 (2010).
11. Fu, Y. & Galan, J. E. A *Salmonella* protein antagonizes Rac-1 and Cdc42 to mediate host-cell recovery after bacterial invasion. *Nature* **401**, 293–297 (1999).
12. Sun, H., Kamanova, J., Lara-Tejero, M. & Galán, J. A family of *Salmonella* type III secretion effector proteins selectively targets the NF-κB signaling pathway to preserve host homeostasis. *PLoS Pathog.* **12**, e1005484 (2016).
13. Jones, M. A. et al. Secreted effector proteins of *Salmonella* dublin act in concert to induce enteritis. *Infect. Immun.* **66**, 5799–5804 (1998).
14. Zhang, S. et al. The *Salmonella enterica* serotype Typhimurium effector proteins SipA, SopA, SopB, SopD, and SopE2 act in concert to induce diarrhea in calves. *Infect. Immun.* **70**, 3843–3855 (2002).
15. Wall, A. et al. Small GTPase Rab8a-recruited phosphatidylinositol 3-kinase γ regulates signaling and cytokine outputs from endosomal Toll-like receptors. *J. Biol. Chem.* **292**, 4411–4422 (2017).
16. Luo, L. et al. TLR crosstalk activates LRP1 to recruit Rab8a and PI3Kγ for suppression of inflammatory responses. *Cell Rep.* **24**, 3033–3044 (2018).
17. Tong, S., Wall, A., Hung, Y., Luo, L. & Stow, J. Guanine nucleotide exchange factors activate Rab8a for Toll-like receptor signalling. *Small GTPases* **12**, 27–43 (2021).
18. Brumell, J. et al. SopD2 is a novel type III secreted effector of *Salmonella* Typhimurium that targets late endocytic compartments upon delivery into host cells. *Traffic* **4**, 36–48 (2003).
19. Spanò, S., Gao, X., Hannemann, S., Lara-Tejero, M. & Galán, J. A bacterial pathogen targets a host Rab-Family GTPase defense pathway with a GAP. *Cell Host Microbe* **19**, 216–226 (2016).
20. Creagh, E. & O'Neill, L. TLRs, NLRs and RLRs: a trinity of pathogen sensors that co-operate in innate immunity. *Trends Immunol.* **27**, 352–357 (2006).
21. Lee, J., Mo, J., Shen, C., Rucker, A. & Raz, E. Toll-like receptor signaling in intestinal epithelial cells contributes to colonic homoeostasis. *Curr. Opin. Gastroenterol.* **23**, 27–31 (2007).
22. Kelly, D., Conway, S. & Aminov, R. Commensal gut bacteria: mechanisms of immune modulation. *Trends Immunol.* **26**, 326–333 (2005).
23. Eckmann, L. Sensor molecules in intestinal innate immunity against bacterial infections. *Curr. Opin. Gastroenterol.* **22**, 95–101 (2006).
24. Shibolet, O. & Podolsky, D. TLRs in the Gut. IV. Negative regulation of Toll-like receptors and intestinal homeostasis: addition by subtraction. *Am. J. Physiol. Gastrointest. Liver Physiol.* **292**, G1469–G1473 (2007).
25. Lang, T. & Mansell, A. The negative regulation of Toll-like receptor and associated pathways. *Immunol. Cell Biol.* **85**, 425–434 (2007).
26. Hardt, W.-D., Chen, L.-M., Schuebel, K. E., Bustelo, X. R. & Galán, J. E. *Salmonella* Typhimurium encodes an activator of Rho GTPases that induces membrane ruffling and nuclear responses in host cells. *Cell* **93**, 815–826 (1998).
27. Zhou, D., Chen, L. M., Hernandez, L., Shears, S. B. & Galan, J. E. A *Salmonella* inositol polyphosphatase acts in conjunction with other bacterial effectors to promote host cell actin cytoskeleton rearrangements and bacterial internalization. *Mol. Microbiol.* **39**, 248–259 (2001).
28. Sato, T. et al. Rab8a and Rab8b are essential for several apical transport pathways but insufficient for ciliogenesis. *J. Cell Sci.* **127**, 422–431 (2014).
29. Steele-Mortimer, O. et al. Activation of Akt/protein kinase B in epithelial cells by the *Salmonella* Typhimurium effector sigD. *J. Biol. Chem.* **275**, 37718–37724 (2000).
30. Marcus, S., Wenk, M., Steele-Mortimer, O. & Finlay, B. A synaptojanin-homologous region of *Salmonella* Typhimurium SigD is essential for inositol phosphatase activity and Akt activation. *FEBS Lett.* **494**, 201–207 (2001).
31. Pereira-Leal, J. B. & Seabra, M. C. The mammalian Rab family of small GTPases: definition of family and subfamily sequence motifs suggests a mechanism for functional specificity in the Ras superfamily. *J. Mol. Biol.* **301**, 1077–1087 (2000).
32. Pereira-Leal, J. B. & Seabra, M. C. Evolution of the Rab family of small GTP-binding proteins. *J. Mol. Biol.* **313**, 889–901 (2001).
33. D'Costa, V. et al. *Salmonella* disrupts host endocytic trafficking by SopD2-mediated inhibition of Rab7. *Cell Rep.* **12**, 1508–1518 (2015).
34. Guo, Z., Hou, X., Goody, R. S. & Itzen, A. Intermediates in the guanine nucleotide exchange reaction of Rab8 protein catalyzed by guanine nucleotide exchange factors rabin8 and GRAB. *J.Biol.Chem.* **288**, 32466–32474 (2013).
35. Hattula, K., Furuhjelm, J., Arffman, A. & Peränen, J. A Rab8-specific GDP/GTP exchange factor is involved in actin remodeling and polarized membrane transport. *Mol. Biol. Cell* **13**, 3268–3280 (2002).
36. Homma, Y. & Fukuda, M. Rabin8 regulates neurite outgrowth in both GEF activity-dependent and -independent manners. *Mol. Biol. Cell* **27**, 2107–2118 (2016).
37. Müller, M. & Goody, R. Molecular control of Rab activity by GEFs, GAPs and GDI. *Small GTPases* **9**, 5–21 (2018).
38. Cherfils, J. & Zeghouf, M. Regulation of small GTPases by GEFs, GAPs, and GDIs. *Physiol. Rev.* **93**, 269–309 (2013).
39. Collins, R. "Getting it on"—GDI displacement and small GTPase membrane recruitment. *Mol. Cell* **12**, 1064–1066 (2003).
40. Sivars, U., Aivazian, D. & Pfeffer, S. Yip3 catalyses the dissociation of endosomal Rab–GDI complexes. *Nature* **425**, 856–859 (2003).
41. Yamashita, T. & Tohyama, M. The p75 receptor acts as a displacement factor that releases Rho from Rho-GDI. *Nat. Neurosci.* **6**, 461–467 (2003).
42. Hoiseth, S. K. & Stocker, B. A. Aromatic-dependent *Salmonella* Typhimurium are non-virulent and effective as live vaccines. *Nature* **291**, 238–239 (1981).
43. Kaniga, K., Bossio, J. C. & Galan, J. E. The *Salmonella* Typhimurium invasion genes *invF* and *invG* encode homologues of the AraC and PulD family of proteins. *Mol. Microbiol.* **13**, 555–568 (1994).
44. Demarre, G. et al. A new family of mobilizable suicide plasmids based on broad host range R388 plasmid (IncW) and RP4 plasmid (IncPα) conjugative machineries and their cognate *Escherichia coli* host strains. *Res. Microbiol.* **156**, 245–255 (2005).
45. Gibson, D. et al. Enzymatic assembly of DNA molecules up to several hundred kilobases. *Nat. Methods* **6**, 343–345 (2009).
46. Kabsch, W. XDS. *Acta Crystallogr. D* **66**, 125–132 (2010).
47. Collaborative Computational Project, Number 4. The CCP4 suite: programs for protein crystallography. *Acta Crystallogr. D* **50**, 760–763 (1994).
48. Emsley, P. & Cowtan, K. Coot: model-building tools for molecular graphics. *Acta Crystallogr. D* **60**, 2126–2132 (2004).
49. Adams, P. et al. PHENIX: a comprehensive Python-based system for macromolecular structure solution. *Acta Crystallogr. D* **66**, 213–221 (2010).
50. DeLano, W. L. The PyMOL Molecular Graphics System (2002); http://www.pymol.org
51. Itzen, A., Rak, A. & Goody, R. Sec2 is a highly efficient exchange factor for the Rab protein Sec4. *J. Mol. Biol.* **365**, 1359–1367 (2007).
52. Galán, J. E. & Curtiss III, R. Cloning and molecular characterization of genes whose products allow *Salmonella* Typhimurium to penetrate tissue culture cells. *Proc. Natl Acad. Sci. USA* **86**, 6383–6387 (1989).
53. Chang, S., Song, J. & Galán, J. Receptor-mediated sorting of typhoid toxin during its export from *Salmonella* Typhi-infected cells. *Cell Host Microbe* **20**, 682–689 (2016).
54. Ran, F. A. et al. Genome engineering using the CRISPR–Cas9 system. *Nat. Protoc.* **8**, 2281–2308 (2013).
55. Lara-Tejero, M. et al. Role of the caspase-1 inflammasome in *Salmonella* Typhimurium pathogenesis. *J. Exp. Med.* **203**, 1407–1412 (2006).

Acknowledgements

We thank J. Wang (Tsinghua University, China) for suggestions on structure data processing; the staff of the BL17U1 and BL19U1 beamlines of the National Facility for Protein Science Shanghai (NFPS) at Shanghai Synchrotron Radiation Facility (SSRF) for assistance during data collection; and X. Li (Shandong University, Core facilities for life and environmental sciences) for help with the XRD. Work in X.G.'s laboratory was supported by the National Key R&D Program of China (no. 2018YFE0113000), the National Natural Science Foundation of China (nos. 31770143 and 31901943), the Major Basic Program of Natural Science Foundation of Shandong Province (no. ZR2019ZD21), the Youth Interdisciplinary Innovative Research Group of Shandong University (no. 2020QNQT009) and the Taishan Young Scholars Program (no. tsqn20161005). Work in J.E.G.'s laboratory was supported by NIH grants (nos. R01AI055472 and R01AI079022).

Author contributions

H.L. performed all of the functional analyses, animal and cell biological experiments. K.J., M.T. and Z.C. carried out the biochemical characterization of SopD and solved its crystal structure bound to Rab8. J.E.G. and X.G. supervised the study. J.E.G. and X.G. wrote the paper with comments from all of the authors.

Competing interests

The authors declare no competing interests.

Additional information

Extended data is available for this paper at https://doi.org/10.1038/s41564-021-00866-3.

Supplementary information The online version contains supplementary material available at https://doi.org/10.1038/s41564-021-00866-3.

Correspondence and requests for materials should be addressed to J.E.G. or X.G.

Peer review information: *Nature Microbiology* thanks Samuel Miller, Laurent Terradot and the other, anonymous, reviewer(s) for their contribution to the peer review of this work.

Reprints and permissions information is available at www.nature.com/reprints.

Publisher's note Springer Nature remains neutral with regard to jurisdictional claims in published maps and institutional affiliations.

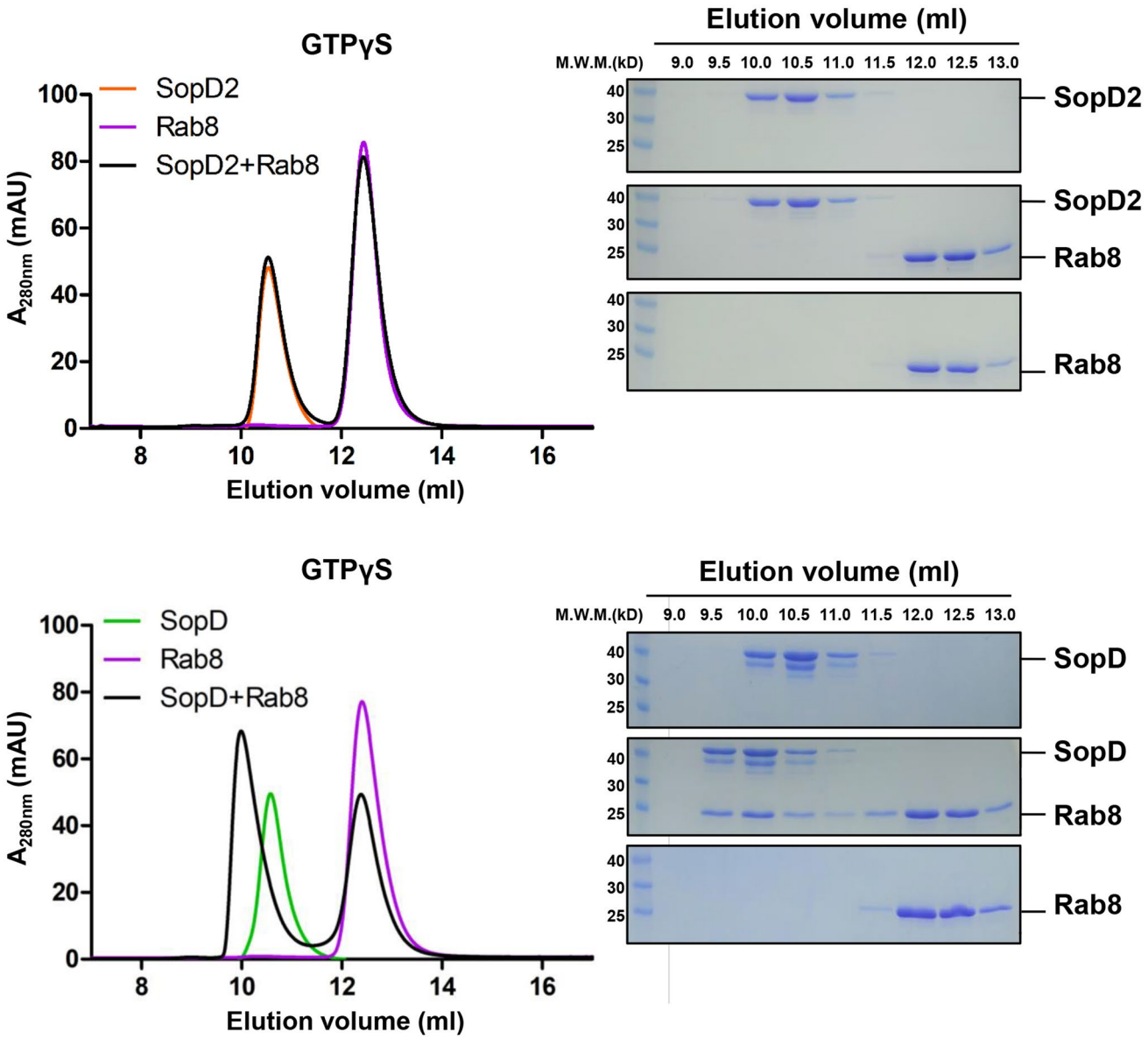

Extended Data Fig. 1 | Size-exclusion chromatography analyses of Rab8 in the presence of SopD or SopD2. Purified Rab8$^{1-183}$ preloaded with GTPγS was incubated with purified SopD or SopD2 and subjected to size-exclusion chromatography in a Superdex 75 increase column. Elution profiles along with SDS-PAGE analyses of the elution fractions are shown. This experiment was conducted at least three times with equivalent results.

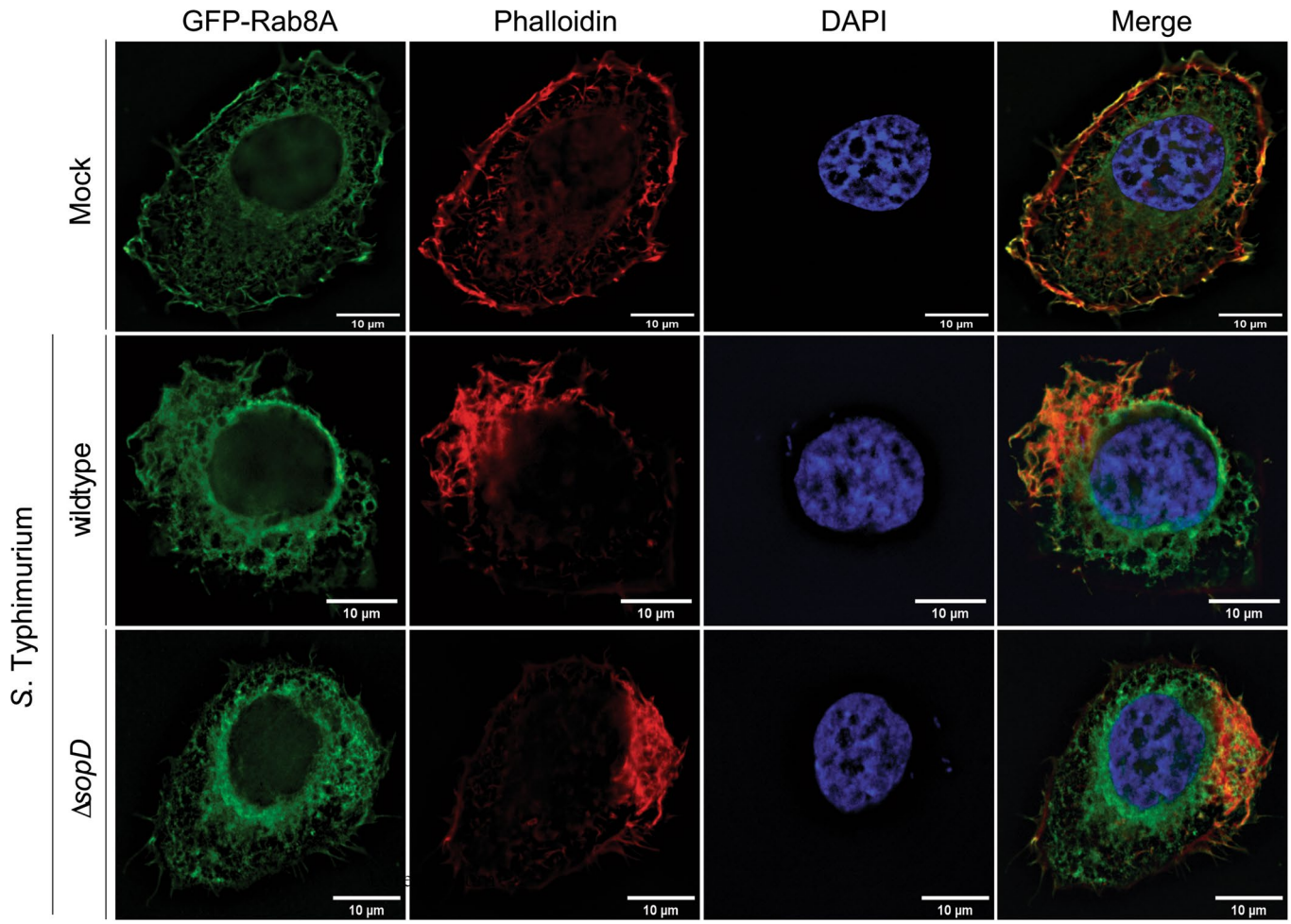

Extended Data Fig. 2 | Rab8 is recruited to the *Salmonella*-induced membrane ruffles. Henle-407 cells were transiently transfected with a plasmid expressing GFP-Rab8A and subsequently infected with wild-type *S.* Typhimurium, its Δ*sopD* isogeneic mutant, or left uninfected (mock). Fifteen minutes after infection, cells were fixed and stained with anti-GFP antibody, to visualize Rab8A (green), rhodamine-labelled Phalloidin, to visualize the actin cytoskeleton (red), and 4′,6-diamidino-2-phenylindole (DAPI) to visualize nuclear and bacteria DNA (blue). Scale bar: 10 μm. This experiment was conducted at least three times with equivalent results.

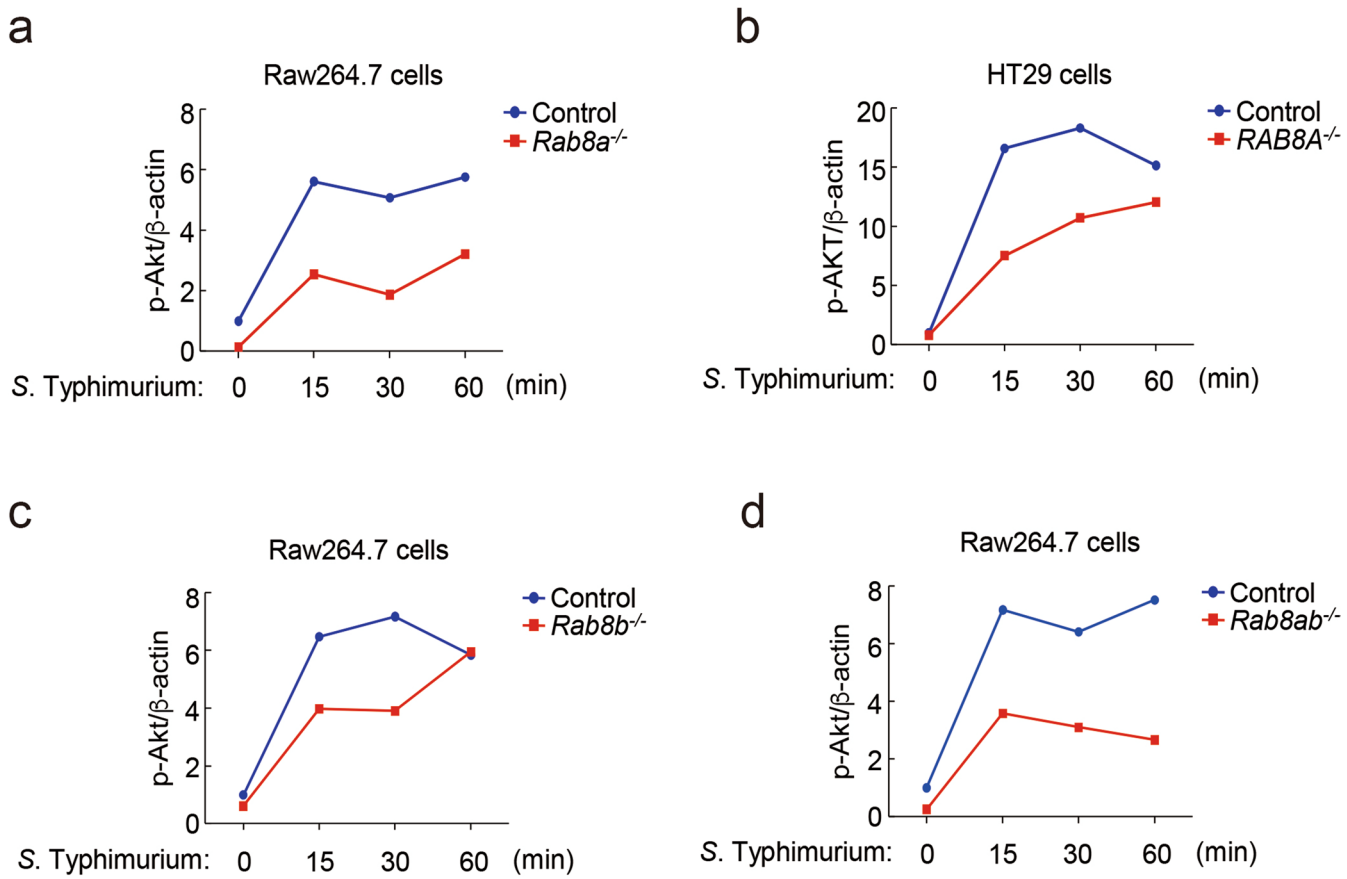

Extended Data Fig. 3 | Rab8 negatively modulates *Salmonella*-induced pro-inflammatory signaling. Effects of Rab8a (**a** and **b**), Rab8b (**c**), or Rab8ab (**d**) deficiency on *S.* Typhimurium-induced AKT activation. Control or deficient Raw264.7 or HT29 (as indicated) cells were infected with wild-type *S.* Typhimurium with a multiplicity of infection of 2 and 10, respectively, and at the indicated times after infection, the levels of phosphorylated Akt were determined by immunoblotting analyses as indicated in Materials and Methods. Values are normalized to the β-actin signal, which served as a loading control. The western blots for this experiment are shown in Fig. 2.

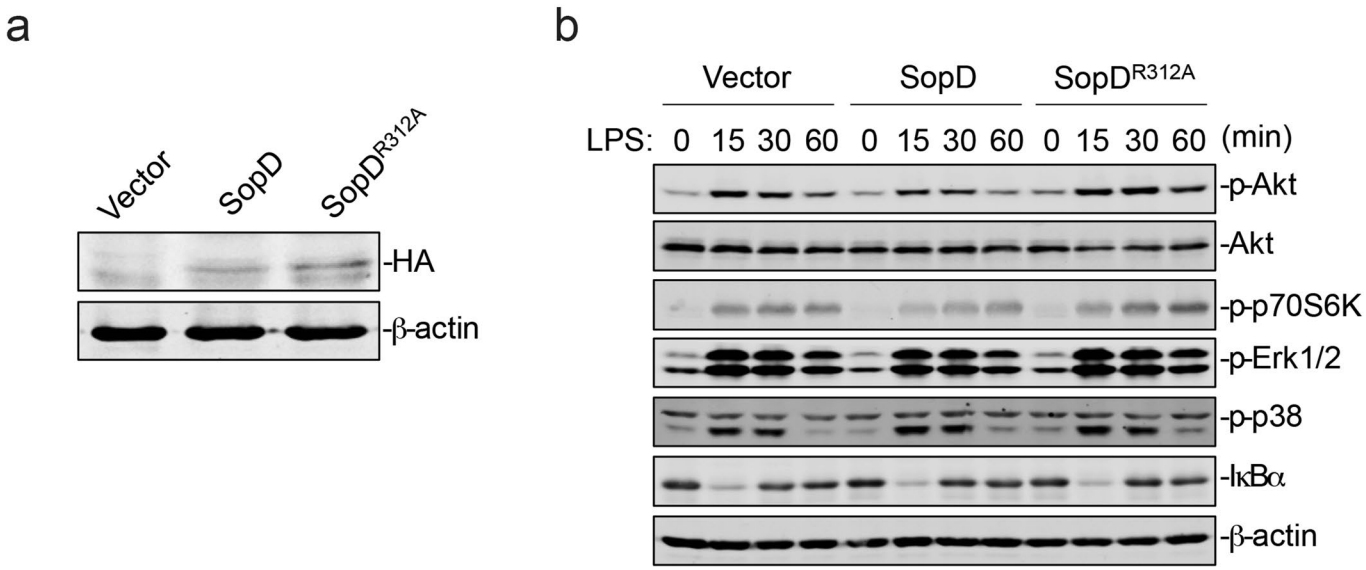

Extended Data Fig. 4 | SopD enhances pro-inflammatory signaling by antagonizing Rab8 through its GAP activity. (**a**) Expression levels of SopD and its catalytic mutant SopD^{R312A} in stable cell lines (Raw264.7). Stable cell lines (Raw264.7) expressing HA-tagged SopD or SopD^{R312A} were lysed before immunoblotting analysis with the antibodies directed to the HA tag and to β-actin (as a loading control). (**b**) Effect of the expression of SopD or its catalytic mutant SopD^{R312A} on LPS-induced activation of AKT, p70S6K, Erk1/2, and p38 MAP, and NF-κB signaling pathways. Raw264.7 cells stably expressing HA-tagged SopD or its GAP-deficient mutant SopD^{R312A} were treated with LPS (100 ng/ml) for the indicated times, lysed, and analyzed by immunoblotting with antibodies specific for the phosphorylated state of AKT, p70S6K, p38, and Erk1/2, as well as an antibody to I-κBα and β-actin (as a loading control). The quantification of the western blot analyses is shown on Fig. 2e.

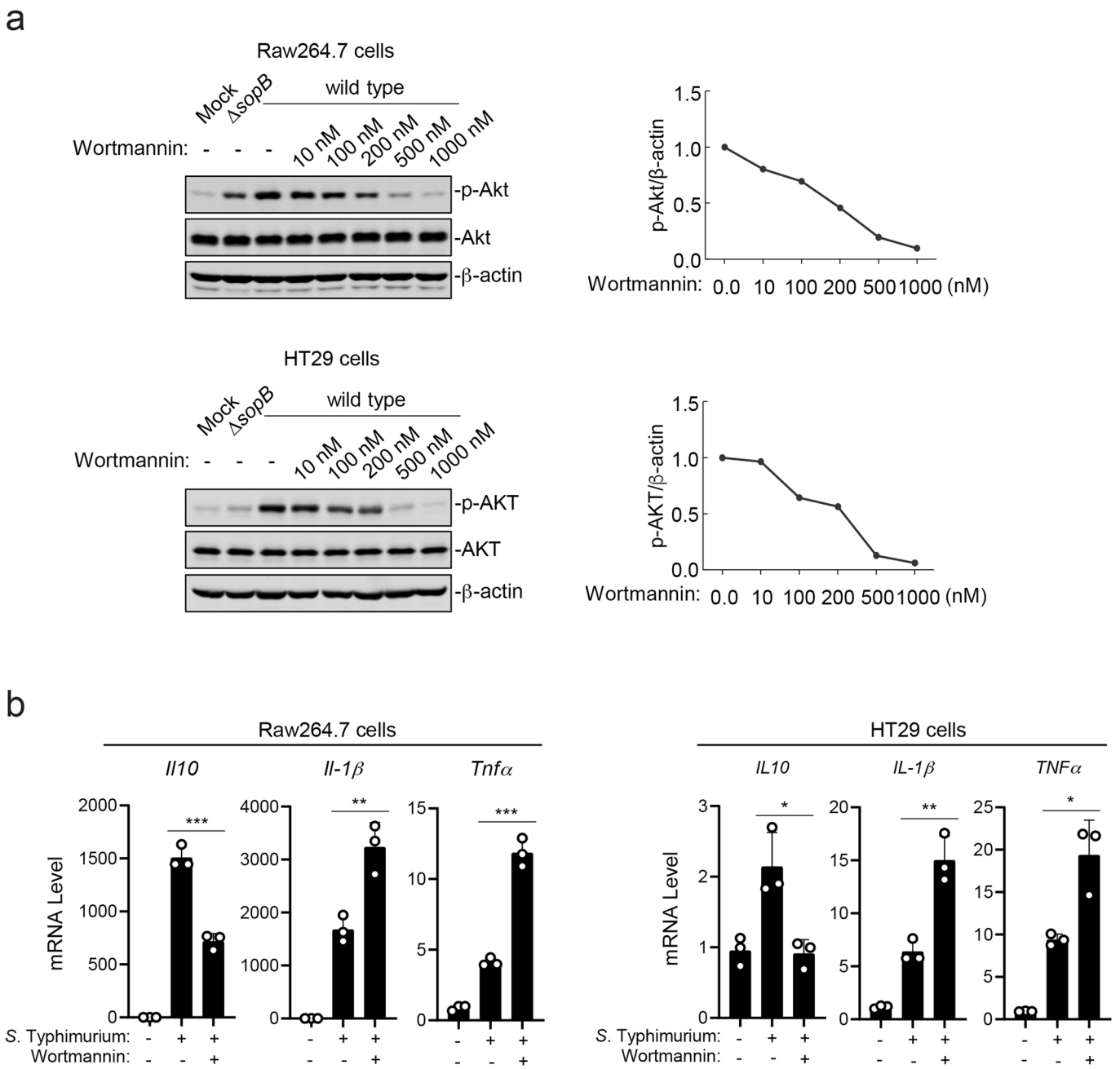

Extended Data Fig. 5 | PI3-kinase is required for *S.* Typhimurium-induced signaling. (**a**) Effects of the PI3-kinase inhibitor Wortmannin on *S.* Typhimurium-induced phosphorylation of AKT. Raw264.7 (MOI=2) or HT29 cells (MOI=10) were pre-treated with increasing concentrations of Wortmannin (10 nM to 1000 nM) for 30 min. Cells were then infected with wild-type *S.* Typhimurium for 30 min and cell lysates were analyzed by immunoblotting with antibodies directed to the phosphorylated (activated) form of Akt or β-actin (as a loading control). Controls included cells left uninfected or infected with the Δ*sopB S.* Typhimurium mutant strain, which is defective for the activation of AKT. Quantification of the immunoblots is shown on the right panels. (**b**) Effects of the PI3-kinase inhibitor Wortmannin on *S.* Typhimurium-induced transcription of cytokine genes. Raw264.7 cells (MOI=5) and HT29 cells (MOI=20) were pre-treated with Wortmannin (100 nM) for 30 min. Cells were left uninfected or infected with wild-type *S.* Typhimurium for 4 hs and the cytokine mRNA levels were measured by qPCR assay. Data are the mean ± standard deviation of three independent experiments. ** $P < 0.01$, *** $P < 0.001$ (unpaired two-sided *t* test).

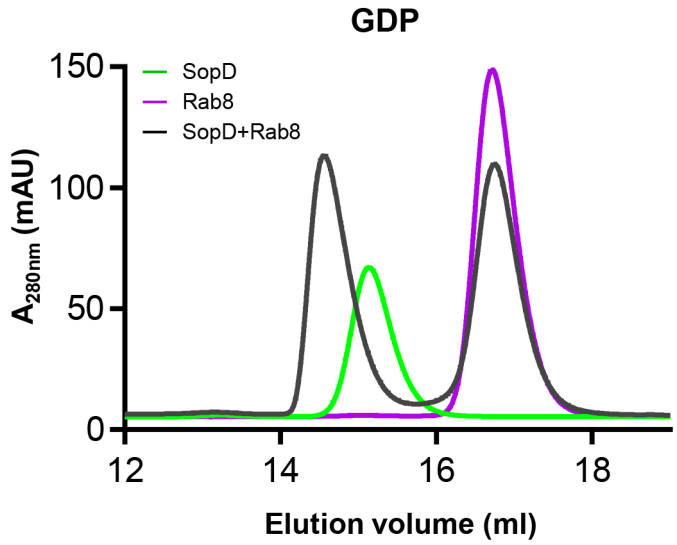

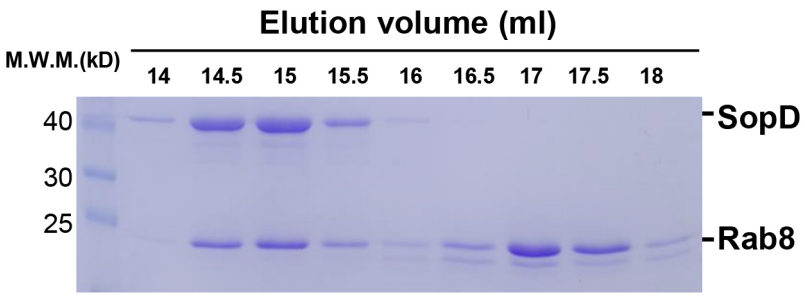

Extended Data Fig. 6 | Size-exclusion chromatography profile of SopD/GDP-bound Rab8 complex. Rab8$^{1-183}$ preloaded with GDP was incubated with SopD, and subjected to size-exclusion chromatography with Superdex 200 increase column. The elution profile along with the SDS-PAGE analyses of the elution fractions of the SopD/Rab8 complex are shown. This experiment was conducted at least three times with equivalent results.

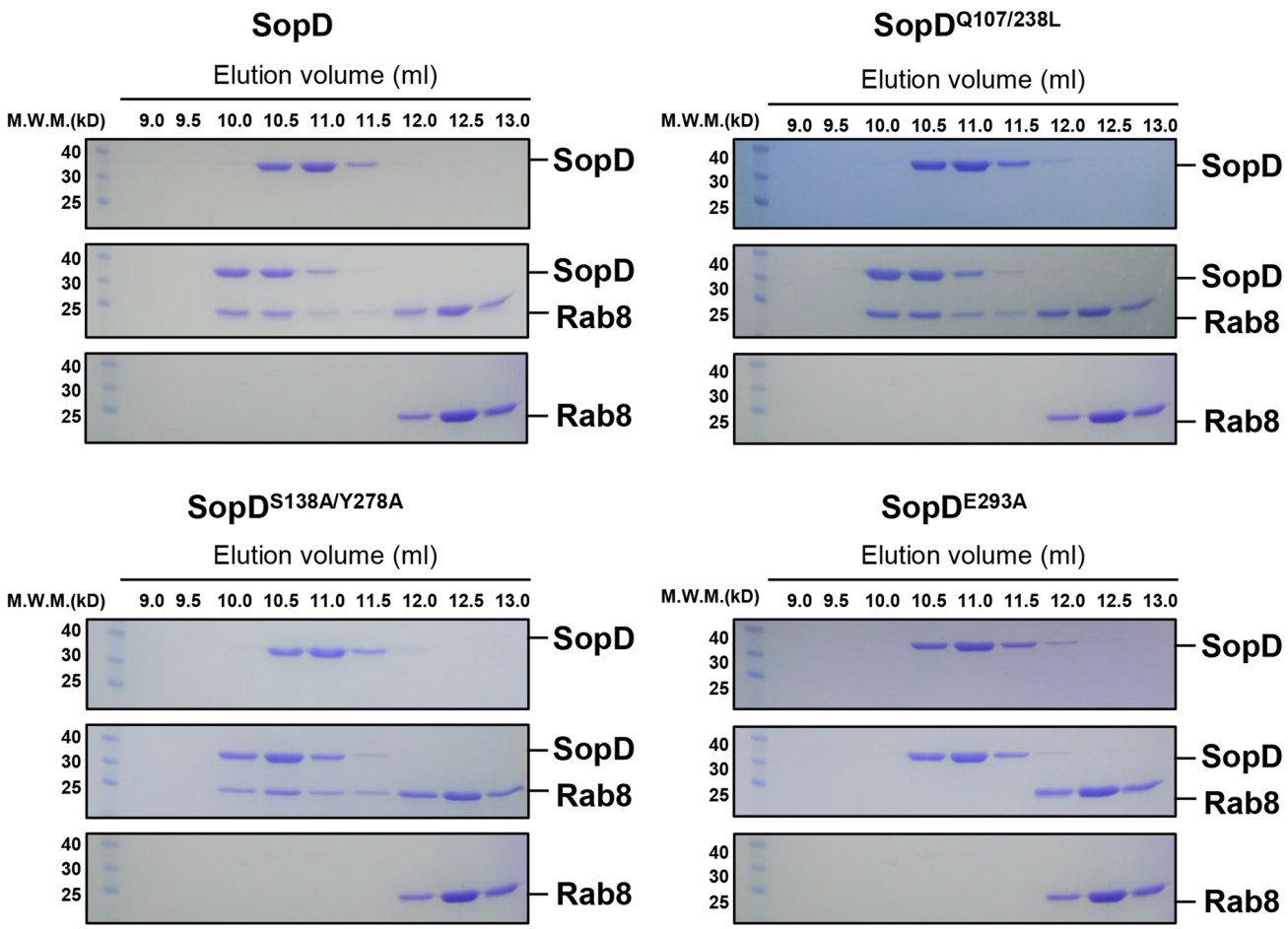

Extended Data Fig. 7 | SDS-PAGE analyses of the elution fractions of the size-exclusion chromatography analyses of SopD carrying mutations in amino acids defining its interface with Rab8. Purified Rab8a$^{1-183}$ preloaded with GDP was incubated with purified SopD or the indicated SopD mutants and subjected to size-exclusion chromatography (see the chromatographic profile in Fig. 3e). Fractions were collected, separated on an SDS-PAGE, and stained with Coomassie blue. This experiment was conducted at least three times with equivalent results.

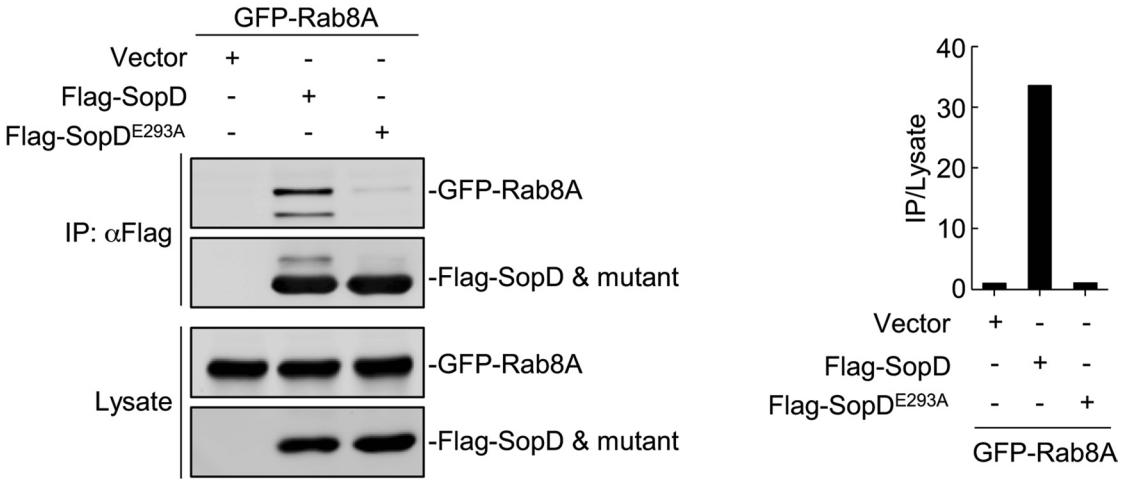

Extended Data Fig. 8 | The SopD^{E293A} mutation disrupts the ability of SopD to form a complex with Rab8. FLAG-epitope tagged SopD or SopD^{E293A} were co-expressed with GFP-Rab8 or empty vector in HEK-293T cells. The cell lysates were co-immunoprecipitated with anti-FLAG M2 beads followed by immunoblotting with anti-GFP and anti-Flag antibodies. The quantification of the intensity of the bands is shown in the right panel. This experiment was conducted at least three times with equivalent results.

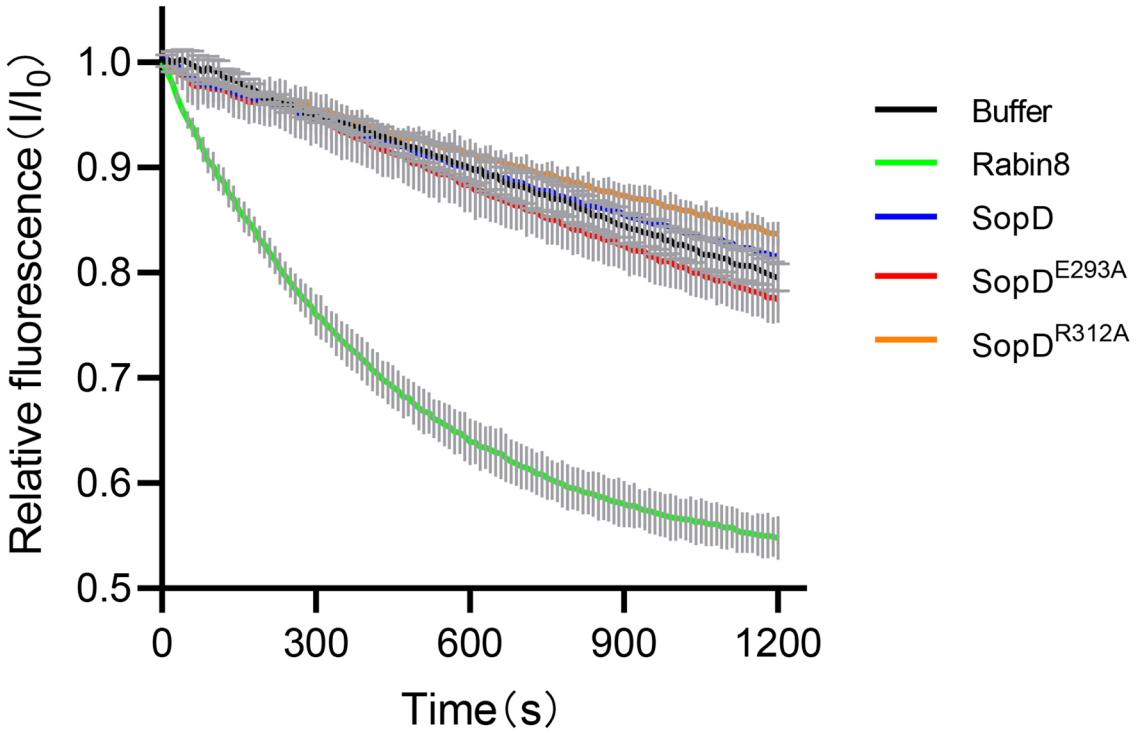

Extended Data Fig. 9 | SopD lacks guanine-nucleotide exchange activity. Mant-GDP-loaded Rab8a (2 μM) was incubated with Rabin8 (0.4 μM) (positive control), SopD (2 μM), 2 μM SopD^{R312A} (2 μM), SopD^{E293A} (2 μM) or buffer only (negative control), in the presence of 5 μM GTPγS. The decreased fluorescence as a result of the mant-GDP to GTPγS exchange was monitored over time. Data are expressed as the mean ± SD from three independent experiments.

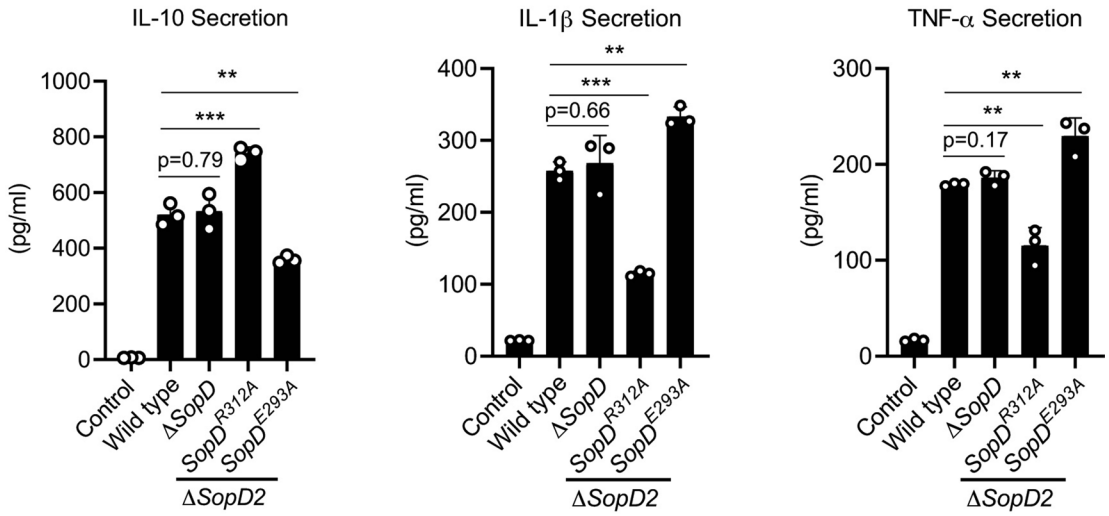

Extended Data Fig. 10 | Effect of SopD or its mutants on cytokine production in *S.* Typhimurium-infected cells. Raw264.7 cells were infected with the indicated *S.* Typhimurium strains (MOI=5) and 18 hours after infection, the levels of the indicated cytokines in cell supernatants were quantified by ELISA. Values are the mean ± SD of three independent measurements. ** $P < 0.01$, *** $P < 0.001$, ns: not significant (unpaired two-sided *t* test).

nature research

Corresponding author(s): Jorge E. Galán

Last updated by author(s): November 30, 2020

Reporting Summary

Nature Research wishes to improve the reproducibility of the work that we publish. This form provides structure for consistency and transparency in reporting. For further information on Nature Research policies, see our Editorial Policies and the Editorial Policy Checklist.

Statistics

For all statistical analyses, confirm that the following items are present in the figure legend, table legend, main text, or Methods section.

n/a	Confirmed	
☐	☒	The exact sample size (*n*) for each experimental group/condition, given as a discrete number and unit of measurement
☐	☒	A statement on whether measurements were taken from distinct samples or whether the same sample was measured repeatedly
☐	☒	The statistical test(s) used AND whether they are one- or two-sided *Only common tests should be described solely by name; describe more complex techniques in the Methods section.*
☐	☒	A description of all covariates tested
☐	☒	A description of any assumptions or corrections, such as tests of normality and adjustment for multiple comparisons
☐	☒	A full description of the statistical parameters including central tendency (e.g. means) or other basic estimates (e.g. regression coefficient) AND variation (e.g. standard deviation) or associated estimates of uncertainty (e.g. confidence intervals)
☐	☒	For null hypothesis testing, the test statistic (e.g. *F*, *t*, *r*) with confidence intervals, effect sizes, degrees of freedom and *P* value noted *Give P values as exact values whenever suitable.*
☒	☐	For Bayesian analysis, information on the choice of priors and Markov chain Monte Carlo settings
☒	☐	For hierarchical and complex designs, identification of the appropriate level for tests and full reporting of outcomes
☒	☐	Estimates of effect sizes (e.g. Cohen's *d*, Pearson's *r*), indicating how they were calculated

Our web collection on statistics for biologists contains articles on many of the points above.

Software and code

Policy information about availability of computer code

Data collection	Odissey v3.0 software package (LI-COR)
Data analysis	XDS Kabsch, 2010 http://xds.mpimf-heidelberg.mpg.de/;CCP Dodson et al., 1997 http;//www.ccp4.ac.uk/; [HENIX Adams et al., 2010 https://www.phenix-online.org/; Coot Emsley et al., 2010 https:www2.mrc-lamb.cam.ac.uk/personal/pemsley/coot/; PyMOL The PyMOL Molecular Graphics System, Schrodiner https://pymol.org/2/; Prism 8 GraphPad https://www.graphpad.com/scientific-software/prism

For manuscripts utilizing custom algorithms or software that are central to the research but not yet described in published literature, software must be made available to editors and reviewers. We strongly encourage code deposition in a community repository (e.g. GitHub). See the Nature Research guidelines for submitting code & software for further information.

Data

Policy information about availability of data

All manuscripts must include a data availability statement. This statement should provide the following information, where applicable:

- Accession codes, unique identifiers, or web links for publicly available datasets
- A list of figures that have associated raw data
- A description of any restrictions on data availability

all data associated with this paper is provided in the paper except the coordinates of the atomic structure which have been deposited in the Protein Data Bank with the accession code 7BWT

Field-specific reporting

Please select the one below that is the best fit for your research. If you are not sure, read the appropriate sections before making your selection.

☒ Life sciences ☐ Behavioural & social sciences ☐ Ecological, evolutionary & environmental sciences

For a reference copy of the document with all sections, see nature.com/documents/nr-reporting-summary-flat.pdf

Life sciences study design

All studies must disclose on these points even when the disclosure is negative.

Sample size	Sample si zes were empirica ll y determined to optimize numb ers based on our previous experience with equiva lent experiments [see for example Sun et al. Nature Microbiol. 3:1122-1130 (2018)]
Data exclusions	No data were excluded
Replication	All findings described here were confirmed by repeating experiments as indicated in the figure legends and, when possible/ applicable , performing distinct experiments to support the same experimental finding.
Randomization	Where applicable, samples and animals were randomly allocated into the different groups.
Blinding	Investigators were not blinded to group allocation during the experiments or to the outcome assessment as it was not practical to do so.

Reporting for specific materials, systems and methods

We require information from authors about some types of materials, experimental systems and methods used in many studies. Here, indicate whether each material, system or method listed is relevant to your study. If you are not sure if a list item applies to your research, read the appropriate section before selecting a response.

Materials & experimental systems

n/a	Involved in the study
☐	☒ Antibodies
☐	☒ Eukaryotic cell lines
☒	☐ Palaeontology and archaeology
☐	☒ Animals and other organisms
☒	☐ Human research participants
☒	☐ Clinical data
☒	☐ Dual use research of concern

Methods

n/a	Involved in the study
☒	☐ ChIP-seq
☒	☐ Flow cytometry
☒	☐ MRI-based neuroimaging

Antibodies

Antibodies used

Mouse monoclonal anti-Flag MBL Cat# M185-3L (use at 1:2000)
Mouse monoclonal anti-Flag Sigma Cat# F3165 (use at 1:2000)
Mouse monoclonal anti-GFP MBL Cat# M048-3 (use at 1:5000)
Mouse monoclonal anti-HA MBL Cat# M180-3 (use at 1:5000)
Mouse monoclonal anti-His ABclonal Cat# AE003 (use at 1:5000)
Mouse monoclonal anti-HA Biolegend Cat# 901501 (use at 1:2000)
Mouse monoclonal anti-IκBα Cell Signaling Techno logy Cat# 4814S (use at 1:1000)
Rabbit polyclonal anti-β-actin Sigma Cat# A2066 (use at 1:3000)
Rabbit polyclonal anti-GFP In vitrogen Cat# A6455 (use at i:2000)
Rabbit polyclonal anti-AKT Cell Signaling Technology Cat# 9272 (use at 1:1000)
Rabbit polyclonal anti-phospho-p38 Cell Signaling Technology Cat# 9211S (use at 1:1000)
Rabbit monoclonal anti-phospho-AKT Cell Signaling Technology Cat# 4060T (use at 1:2000)
Rabbit monoclonal anti-phospho-ERKl/2 Cell Signaling Technology Cat# 4370S (use at 1:2000)
Rabbit monoclonal anti-phospho-p70 S6 Kinase Cell Signaling Technology Cat# 9234T (use at 1:1000)
Goat polyclonal anti-mouse lgG, HRP conjugated MBL Cat# 330 (use at 1:5000)
Rabbit monoclonal anti-mouse (li ght chain specific) lgG, HRP conjugated CST Cat# 58802 (use at 1:3000)
Rabbit polyclonal anti-mouse IgG DyLight conjugated, Thermo Fisher Cat# SA5-35521 (use at 1:10,000)

Validation

When possible, antibodies were validated by including positive and/or negative controls in the experiments themselves. Otherwise, we relied on the validation data provided by the supplier.

Eukaryotic cell lines

Policy information about cell lines

Cell line source(s)	Henle-407 human epithelial cell line obtained from the Roy Curtiss laboratory collection; HEK-293T, raw264.7, and HT29 cells were obtained from the ATCC.
Authentication	The cells were frequently checked for their morphological features, growth properties and functionalities.
Mycoplasma contamination	Cells were routinely tested for Mycoplasma contamination and in all cases the cells tested negative.
Commonly misidentified lines (See ICLAC register)	No commonly misidentified cell lines were used.

Animals and other organisms

Policy information about studies involving animals; ARRIVE guidelines recommended for reporting animal research

Laboratory animals	A mix of male and female 6-10 week old C57BL/6 mice carrying a wild type allele of NRAMP-1 were used in this study.
Wild animals	No wild animals were used in this study
Field-collected samples	No field-collected samples were used in these studies
Ethics oversight	All animal experiments followed the ethical regulations and were conduced according to protocols approved by the Yale University's Institutional Animal Care and Use Committee

Note that full information on the approval of the study protocol must also be provided in the manuscript.